



# The spectroscopic (FT-IR, FT-Raman, dispersive Raman and NMR) study of ethyl-6-chloronicotinate molecule by combined density functional theory



Mehmet Karabacak<sup>a</sup>, Zuhre Calisir<sup>b</sup>, Mustafa Kurt<sup>b</sup>, Etem Kose<sup>c</sup>, Ahmet Atac<sup>c,\*</sup>

<sup>a</sup> Department of Mechatronics Engineering, H.F.T. Technology Faculty, Celal Bayar University, Turgutlu, Manisa, Turkey

<sup>b</sup> Department of Physics, Ahi Evran University, Kirsehir, Turkey

<sup>c</sup> Department of Physics, Celal Bayar University, Manisa, Turkey

## ARTICLE INFO

### Article history:

Received 9 May 2014

Received in revised form 3 September 2015

Accepted 10 September 2015

Available online 21 September 2015

### Keywords:

Ethyl-6-chloro-nicotinate

DFT and TD-DFT

FT-IR

FT-Raman and dispersive Raman spectra

NMR

NLO NBO and MEP

## ABSTRACT

In this study, ethyl-6-chloronicotinate (E-6-CIN) molecule is recorded in the region 4000–400  $\text{cm}^{-1}$  and 3500–100  $\text{cm}^{-1}$  (FT-IR, FT-Raman and dispersive Raman, respectively) in the solid phase.  $^1\text{H}$  and  $^{13}\text{C}$  nuclear magnetic resonance (NMR) spectra are recorded in DMSO solution. The structural and spectroscopic data of the molecule are obtained for two possible isomers (S1 and S2) from DFT (B3LYP) with 6-311++G(d,p) basis set calculations. The geometry of the molecule is fully optimized, vibrational spectra are calculated and fundamental vibrations are assigned on the basis of the potential energy distribution (PED) of the vibrational modes.  $^1\text{H}$  and  $^{13}\text{C}$  NMR chemical shifts are calculated by using the gauge-invariant atomic orbital (GIAO) method. The electronic properties, such as excitation energies, oscillator strengths, wavelengths, HOMO and LUMO energies, are performed by time-dependent density functional theory (TD-DFT). Total and partial density of state and overlap population density of state diagrams analysis are presented for E-6-CIN molecule. Furthermore, frontier molecular orbitals (FMO), molecular electrostatic potential, and thermodynamic features are performed. In addition to these, reduced density gradient of the molecule is performed and discussed. As a conclusion, the calculated results are compared with the experimental spectra of the title compound. The results of the calculations are applied to simulate the vibrational spectra of the molecule, which show excellent agreement with the observed ones. The theoretical and tentative results will give us a detailed description of the structural and physicochemical properties of the molecule. Natural bond orbital analysis is done to have more information stability of the molecule arising from charge delocalization, and to reveal the information regarding charge transfer within the molecules.

© 2015 Elsevier B.V. All rights reserved.

## 1. Introduction

Nicotinate is a very important molecule which has attracted much attention in terms of its wide range of applications. Especially the developments of the areas of the starting materials, reaction technology and the working-up to the final product are examined [1]. Ethyl chloronicotinate is a compound of considerable biological interest. Ethyl 6-chloronicotinate is also known as 6-chloronicotinic acid ethyl ester. It is a nicotinic acid derivative used in the preparation of potent H3 receptor antagonists. A method was determined to measure the percutaneous absorption of radioactive nicotinic acid and ethyl nicotinate in excised human skin by Cronin and Stoughton [2]. Goher et al. [3] synthesized azido complex of ethyl nicotinate; new copper (I) thiocyanato complexes,  $[\text{Cu}(\text{NCS})\text{L}]_n$  (L = methyl nicotinate 1, ethyl nicotinate 2) and  $[\text{HL}][\text{Cu}(\text{NCS})_2]$  (HL = H-ethyl isonicotinate 3), were studied and examined by spectroscopic and crystallographic methods. Structural and spectral study of various complexes of nicotinate derivatives were reported

[4]. The importance of nicotinate is seen especially on health (skin) in the literature [5–7]. The cloning, characterization by genetic complementation, and physical mapping of several *A. caulinodans* nicotinate catabolism genes were reported by Buckmiller et al. [8].

There are some papers related to spectroscopic and synthesized studies for derivatives of nicotinate in the literature [6–10]. The results of the effect of alkali metals on the electronic structure of 2-aminonicotinic acid are shown and the changes of chemical shifts of protons and carbons ( $^1\text{H}$  and  $^{13}\text{C}$  NMR) in the series of alkali metal 2-aminonicotinate were observed [9]. Vibrational structure and antimicrobial activity of selected isonicotinate, potassium picolinate and nicotinate [10] were investigated. The relationship between chemical structure and antimicrobial activity of selected nicotinate, p-iodobenzoates, picolinate and isonicotinate was published by Koczoń et al. [11]. Studies of vibrational and NMR spectra of alkali metal nicotinate were presented [12,13]. The molecular structure of methyl 6-chloronicotinate was reported by Xu et al. [14].

To the best of our knowledge, the analysis of literature showed that no experimental and computational (DFT) spectroscopic study performed on the conformation, vibrational IR, Raman, dispersive Raman

\* Corresponding author.

and NMR spectra of E-6-CIN. This inadequacy has encouraged us to study theoretical and experimental spectroscopic research based on FT-IR, FT-Raman, dispersive Raman, NMR spectra and electronic structure of the title molecule. The theoretical geometrical parameters, IR, Raman and NMR spectra, HOMO–LUMO energies and molecular electrostatic potential of the molecule were performed in the ground state. Moreover, the changes with different temperatures in the thermodynamic functions (the heat capacity, entropy, and enthalpy) were investigated of the present molecule. The nonlinear optical (NLO) properties and global reactivity descriptors of the studied molecule, such as chemical potential, electronegativity, hardness, softness and electrophilicity index, were reported. Reduced density gradient (RDG) of E-6-CIN molecule was graphed and showed related interaction in the molecule. Natural bond orbital (NBO) analysis was done. The results examined by the experiment (FT-IR, FT-Raman, dispersive Raman and NMR spectra) were supported by the computed results, comparing with experimental characterization data; vibrational wavenumbers and chemical shifts values are in fairly good agreement with the experimental results.

## 2. Theoretical calculations

Important appliances to understand the fundamental vibrational properties and the electronic structure of the compound were used in DFT calculations. Because of this reason, the gradient corrected density functional theory (DFT) [15] with the Becke's three-parameter hybrid functional (B3) [16] for the exchange part and the Lee–Yang–Parr (LYP) correlation function [17], were accepted as a cost-effective approach, for the computation of molecular structure, vibrational frequencies and energies of optimized structures by using Gaussian 09 suite of quantum chemical codes [18].

The scan coordinate, selected torsion angle,  $T(O10-C8-C2-C3)$  which is changed every  $10^\circ$  and molecular energy profile is calculated from  $0^\circ$  to  $360^\circ$  including proposed conformers. According to scan program, there are two conformers (S1 and S2) in Fig. S1. Also, they were optimized in the ground state (in vacuum) at DFT by the hybrid B3LYP level of theory using the 6-311++G(d,p) basis set (Fig. 1). The optimized results were used to calculate the spectroscopic features of the title molecule such as: vibrational frequencies, isotropic chemical shifts and electronic properties. To improve and make the calculations agree with the experimental results harmonic frequencies were fixed by scaling factors, 0.983 up to  $1700\text{ cm}^{-1}$  and 0.958 for greater than  $1700\text{ cm}^{-1}$  [19]. The assignments of vibrational frequencies were made on the basis of the corresponding PEDs by using VEDA program [20]. Gaussview program [21] was also considered to get visual animation and also for the verification of the normal modes assignment.

The isotropic chemical shifts are frequently used to aid identification of organic compounds and accurate predictions of molecular geometries. The B3LYP method allows calculating the shielding constants with accuracy and the GIAO method [22,23] is one of the most common approaches for calculating nuclear magnetic shielding tensors. The  $^1\text{H}$  and  $^{13}\text{C}$  NMR isotropic shielding tensors were calculated with the GIAO method by using the optimized parameters obtained from B3LYP/6-311++G(d,p) method.

In order to understand the electronic properties, such as HOMO–LUMO energies, dipole moment, absorption wavelengths, and oscillator strengths were calculated using B3LYP method of the time-dependent DFT (TD-DFT) [24–27] based on the optimized structure. Moreover, to calculate group contributions to the molecular orbitals and to prepare total density of states (TDOS or DOS), the partial density of states (PDOS) and overlap population density of states (OPDOS) spectra GaussSum 2.2 [28] was used. The contribution of a group to a molecular orbital was calculated using Mulliken population analysis. The PDOS and OPDOS spectra were created by convoluting the molecular orbital information with Gaussian curves of unit height and an FWHM (full width at half maximum) of 0.3 eV.

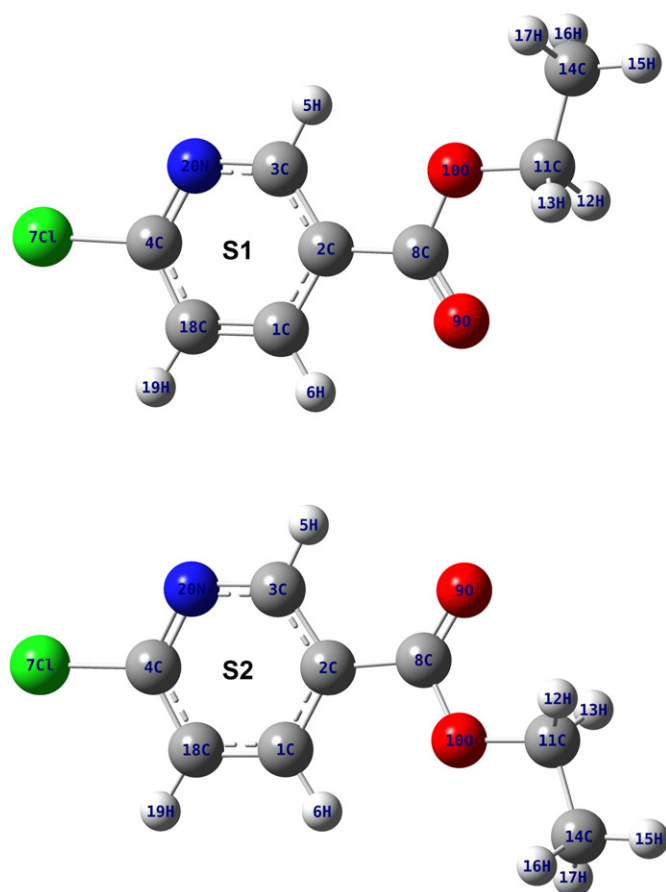


Fig. 1. The theoretical optimized geometric structures of E-6-CIN for S1 and S2 conformers.

The molecular electrostatic potential (MEPs) of the present molecule is illustrated and evaluated. The changes of the heat capacity, entropy, and enthalpy of the title molecule were investigated for the different temperatures (from 100 K to 700 K) from the vibrational frequency calculations in gas phase. To calculate NLO properties (dipole moment, mean polarizability, and first static hyperpolarizability) of the molecule the finite field approach DFT was used. The RDG is performed by Multiwfn [29], and plotted by VMD program [30], respectively. NBO 3.1 program [31] as implemented in the Gaussian 09 [18] package was used for NBO calculations at the DFT/B3LYP level. The NBO calculations were performed to understand varied second order interactions. These interactions were between the occupied orbitals and unoccupied orbitals, which are a measure of the intermolecular delocalization or hyper conjugation.

## 3. Experimental treatments

The compound E-6-CIN in solid phase, with a stated purity of 99%, was obtained from Merck Company, Germany and was used without further purification. The FT-IR spectrum of E-6-CIN molecule was recorded between  $4000$  and  $400\text{ cm}^{-1}$  on a Perkin-Elmer FT-IR System Spectrum BX spectrometer, at room temperature with the spectral resolution of  $4.0\text{ cm}^{-1}$ . FT-Raman spectrum of the compound was obtained in the range of  $3500$ – $100\text{ cm}^{-1}$  using a Bruker RFS 100/S FT-Raman instrument by using  $1064\text{ nm}$  line of Nd: YAG laser as excitation. The detector is a liquid nitrogen cooled Ge detector. The Raman spectrum of the pure compound was measured using a Thermo Fisher Scientific model DXR dispersive Raman instrument using  $780\text{ nm}$  laser excitation in the range of  $3500$ – $100\text{ cm}^{-1}$ . The spectral resolution is  $\pm 5\text{ cm}^{-1}$ . NMR measurements were recorded in Varian Infinity Plus spectrometer at 300 K. The compound was dissolved in DMSO. The chemical shifts

were reported in ppm relative to tetramethylsilane (TMS) for  $^1\text{H}$  and  $^{13}\text{C}$  NMR spectra. NMR spectra were obtained at a base frequency of 600 MHz for  $^1\text{H}$  and 150 MHz for  $^{13}\text{C}$  nuclei.

#### 4. Results and discussion

The optimized geometric parameters (bond lengths and angles), vibrational frequencies (FT-IR, FT-Raman and dispersive Raman), and NMR spectral analysis of the results for the studied molecule were evaluated and experimental and theoretical techniques were analyzed by using quantum chemical calculations in the following sections. In order to investigate the most stable isomer of E-6-CIN, the molecular PES scan is searched and the selected torsion angles  $T(\text{O}10-\text{C}8-\text{C}2-\text{C}3)$  are changed every  $10^\circ$  (from  $10^\circ$  to  $360^\circ$ ) by using B3LYP/6-311++G(d,p) method. The molecular energy profile is calculated including proposed conformers. The conformational analysis of the molecule showed that there are two local minima near  $0^\circ$  (or  $360^\circ$ ) and  $180^\circ$  for E-6-CIN molecule. In other words, according to scan results, there are two possible conformers (S1 and S2). The potential energy curves between the dihedral angles and their corresponding energies are given in Fig. S1. The molecule was optimized considering the result of scan for proposed S1 and S2 conformers. To obtain more stable conformer, the energies of different conformation of the title molecule were calculated with B3LYP/6-311++G(d,p) level. The minimum energies of two structures (S1 and S2) of the title molecule are  $-975.2518775$  and  $-975.2513152$  Hartree, respectively. The proposed two isomers of E-6-CIN molecule energies and energy difference [the relative energy of the other isomer is as follows:  $\Delta E = E(\text{Sn}) - E(\text{S1})$ ]; the isomer S1 is the lowest energy as reference point] are determined in Table 1. According to the DFT calculation of the conformers, the isomer S1 is predicted to be more stable from 0.3528 kcal/mol than the other conformer S2. It is clear that in the conformational analysis the molecule is more stable (S1) for near local minima of  $0^\circ$ . The geometrical structural analysis, vibrational frequencies, NMR chemical shifts and other calculations of the present molecule are depicted based on the most stable structure of the molecule after scanned and optimized, by using 6-311++G(d,p) basis set. That is, we have focused on S1 isomer of E-6-CIN molecule to clarify molecular structure, assignments of vibrational spectra, chemical shifts, and the other theoretical calculations.

##### 4.1. Geometrical structures

E-6-CIN is a substituted pyridine with two different functional groups: a chloro (Cl) atom and ethyl carboxylate group that is planar pyridine ring. The crystal structure of E-6-CIN molecule is not available in the literature until now, because of this reason the geometric parameters, bond lengths and angles, are compared with structurally similar molecule (methyl 6-chloronicotinate) [14]. The scheme of proposed (S1 and S2 isomers) optimized structure of E-6-CIN molecule is shown in Fig. 1. The complete (S1 and S2 isomers) optimized structural parameters of the title molecule are given in Table 2, as matching to the similar structure of experimental values [14] pursuant to the atom numbering scheme in Fig. 1.

**Table 1**  
Calculated energies and energy differences for two possible isomers of E-6-CIN by DFT (B3LYP/6-311++G(d,p)) method.

Conformers	Energy		Energy differences <sup>a</sup>		Point group
	(Hartree)	(kcal/mol)	(Hartree)	(kcal/mol)	
S1	-975.2518775	-611979.8180	0.0000	0.0010	Cs
S2	-975.2513152	-611979.4652	0.0006	0.3528	Cs

<sup>a</sup> Energies of the other conformer relative to the most stable S1 conformer.

Johnson et al. [32] discussed that DFT method predicts bond lengths slightly bigger than experimental values. At a glance from Table 2 optimized C—C bond lengths are generally bigger than experimental data because the molecular geometry of similar molecule in vapor phase may be different from in the solid phase of the title molecule. The C—C bond lengths of the ring are computed in the range of 1.385–1.400 Å for S1 isomer and 1.386–1.400 Å for S2 isomer while the experimental [14] values are observed in the range of 1.367–1.382 Å. The C2—C8 bond is showed that similar behaviors is calculated 0.009 Å larger than the recorded one [14]. The results of CC bond were published in the literature [33] agree well with the results of this study. The bond lengths of ring C—H for the molecule are approximately 0.150 Å bigger than for experimental values of similar structure [14].

The C—X (X; F, Cl, Br ...) bond length indicates a considerable increase when substituted in place of C—H. The C—Cl bond lengths were computed in the range of 1.730–1.751 [34] and 1.755 Å [35] in the substituted chlorine atom with pyridine ring and were observed 1.730 [36] and 1.738 Å [37]. In this study the bond distance C—Cl value is computed at 1.758 Å for two isomers by using B3LYP/6-311G++(d,p) basis set, which is in good agreement with comparing experimental value 1.728 Å [14].

The bond distance values (S1 isomer) of C8=O9, C8—O10 and C11—O10 are calculated at 1.210, 1.345, and 1.452 Å, respectively. The same results are obtained for S2 isomer at 1.209, 1.347, and 1.452 Å, respectively. These values are supported with the experimental 1.198, 1.333, and 1.444 Å, respectively [14]. These bonds were recorded in the literature showing well agree at 1.223, 1.341, and 1.446 Å [38] for ethyl 4-aminobenzoate molecule and calculated as 1.213, 1.356, and 1.448 Å [39] for ethyl p-amino benzoate.

The C—N and C=N bond lengths are predicted as 1.337 Å (1.336 Å for S2 isomer) and 1.317 Å (1.318 Å for S2 isomer), respectively. They are recorded 1.333 and 1.322 Å, respectively [14]. The literatures [34, 35,40,41] are supported with the similar papers for structurally related molecules.

The interaction arises through  $\text{O} \cdots \text{H}$  or  $\text{H} \cdots \text{O}$  two hydrogen-bonded ring ( $\text{O}9 \cdots \text{H}6$  and  $\text{O}10 \cdots \text{H}5$ ) and four hydrogen-bonded  $\text{CH}_x$  groups ( $\text{O}9 \cdots \text{H}12$ ,  $\text{H}13$  and  $\text{O}10 \cdots \text{H}16$ ,  $\text{H}17$ ) in the bonded ring groups are changing increase and decrease as 0.007 and 0.003 Å. Also O—H distances of the bonded  $\text{CH}_x$  groups shortening of the  $\text{O}9 \cdots \text{H}12$ ,  $\text{H}13$  (0.003 Å), while the lengthening of the  $\text{O}10 \cdots \text{H}16$ ,  $\text{H}17$  (0.007 Å) from S1 to S2 isomer. This can effect of location of N atom in the isomers also the dihedral angles of related bonds have redistribution after the changing of N locations. These intramolecular results can see bottom of Table 2.

The ring C—C—C bond angles calculated in the range of 117.2–119.4° correlated with the experimental values but the C1—C2—C3 and C4—C18—C1 bond angles deviated from the normal value ( $120.0^\circ$ ) of the ring; this may be due to the attached chlorine atom at C4 and functional group at C2 atom in the ring, and distorted symmetries and normal values. The calculated bond angles showed the small difference from experimental values; this can be because the calculation belongs to vapor phase and experimental result belongs to solid phase and due to molecules with similar structure was formed. The C—C—N bond angles are found to be a little higher, about  $4^\circ$  to hexagonal angle  $120^\circ$  for the molecule. Moreover, this study concludes that the theoretically calculated bond lengths and bond angles are in well agreement with the earlier studies [34,35,40]. The dihedral angles between the pyridine ring and ethyl carboxylate groups  $\text{C}3-\text{C}2-\text{C}8-\text{O}9 = 180^\circ$ ,  $\text{C}1-\text{C}2-\text{C}8-\text{O}9 = 180^\circ$ , and  $\text{C}11-\text{O}10-\text{C}8-\text{C}2 = 180^\circ$  show good agreement with the literature [42].

##### 4.2. Vibrational spectral analysis

Vibrational spectroscopy can provide an exact measurement of wavelengths of light that are absorbed by a molecule. In this study we investigated frequency calculation analysis to obtain the spectroscopic

Table 2

Bond lengths (Å) and angles (°) experimental and optimized of E-6CIN for S1 and S2 conformers by using B3LYP/6-311++G(d,p).

Bond lengths (Å)	X-ray <sup>a</sup>	S1	S2	Bond angles (°)	X-ray <sup>a</sup>	S1	S2
C1–C2	1.376	1.400	1.400	C2–C1–H6	120.2	119.4	120.1
C1–C18	1.367	1.385	1.386	C18–C1–H6	120.2	121.3	120.7
C2–C3	1.382	1.396	1.397	C4–C18–H19	121.1	120.8	120.8
C2–C8	1.482	1.491	1.490	C1–C18–H19	121.1	122.0	121.9
C3–N20	1.333	1.337	1.336	C17–C4–C18	120.1	118.6	118.6
C4–C17	1.728	1.758	1.758	C17–C4–N20	115.3	116.6	116.6
C4–C18	1.380	1.397	1.397	C1–C2–C8	118.1	118.9	123.3
C4–N20	1.322	1.317	1.318	C3–C2–C8	124.3	123.1	118.7
C8–O9	1.198	1.210	1.209	C2–C8–O9	124.1	123.8	124.1
C8–O10	1.333	1.345	1.347	C2–C8–O10	112.6	112.4	112.1
C11–O10	1.444	1.452	1.452	O9–C8–O10	123.3	123.9	123.8
C11–C14	–	1.514	1.514	C8–O10–C11	116.0	116.5	116.4
C–H ring	0.930	1.082	1.083	O10–C11–H12	109.5	108.4	108.4
C11–H methylene	0.960	1.092	1.092	O10–C11–H13	109.5	108.4	108.4
C14–H methyl	–	1.092	1.092	O10–C11–C14	–	107.6	107.6
Bond angles (°)				H12–C11–H13	109.5	107.9	107.9
C1–C2–C3	117.7	118.0	118.0	H12–C11–C14	–	112.2	112.2
C2–C3–N20	124.2	123.1	123.3	H13–C11–C14	–	112.2	112.2
C3–N20–C4	116.2	117.5	117.4	C11–C14–H15	–	109.5	109.5
N20–C4–C18	124.6	124.8	124.8	C11–C14–H16	–	111.1	111.1
C4–C18–C1	117.8	117.2	117.3	C11–C14–H17	–	111.1	111.1
C18–C1–C2	119.5	119.4	119.2	H15–C14–H16	–	108.2	108.2
C2–C3–H5	117.9	120.6	119.9	H15–C14–H17	–	108.2	108.2
N20–C3–H5	117.9	116.3	116.9	H16–C14–H17	–	108.6	108.6
Intramolecular H bond lengths and dihedral angles							
O9 ··· H6/H5	–	2.541	2.548	H6–C1–C2–C8	–	0.0	0.0
O10 ··· H5/H6	–	2.453	2.450	H5–C3–C2–C8	–	0.0	0.0
O9 ··· H12	–	2.636	2.633	O9–C8–O10–C11	–	0.0	0.0
O9 ··· H13	–	2.636	2.633	C3–C2–C8–O9	–	180.0	180.0
O10 ··· H16	–	2.660	2.660	C1–C2–C8–O9	–	180.0	180.0
O10 ··· H17	–	2.659	2.660	C9–O10–C11–C14	–	180.0	180.0

<sup>a</sup> X-ray data from Ref. [14].

signature of E-6-CIN. The experimental (FT-IR, FT-Raman and dispersive Raman) and calculated wavenumbers at the B3LYP/6-311++G(d,p) and along with assigned vibrational modes of their potential energy distributions (PED) are given in Table 3. The vibrational assignments of the studied molecule have been supported based on Gaussview animation package program [21]. There are differences between the calculated and observed vibrations. Commonly the calculated vibrational wavenumbers are higher than the experimental ones because of the combination of electron correlation effects. Moreover one of the reasons of the differences in calculated wavenumbers has been recorded for free molecule in vacuum, while the experiments were performed for solid sample. Hence in order to improve the agreement with the experimental values, the calculated harmonic wavenumbers were scaled down [19].

The simulated and experimental vibrational (FT-IR and FT-Raman) spectra and also dispersive Raman spectrum of E-6-CIN molecule are shown in Figs. 2–4, respectively. The correlation graphics of the vibrational spectra of E-6-CIN molecule are plotted one by one given in Fig. S2.

The studied molecule E-6-CIN consists of 20 atoms, and so it has 54 normal vibrational modes which are distributed by symmetry species as:  $\Gamma_{\text{vib}} = 35 A' + 19 A''$ . In agreement with  $C_s$  point group symmetry, all vibrations are active both in Raman and infrared spectra. These 54 normal modes have been assigned according to the itemized vibrations of the particular atoms. The intention of this part of the study is to make a comparison with the results saved from the theoretical calculations and related molecules, assigned of the vibrational absorptions. The strong frequencies of them are generally useful to characterize in infrared and Raman spectra. The most important of these to mention is that the stretching vibrational modes are CH, CC, CN, CCl, and CO and in-plane bending modes are CCH, CCC, CCN, CH<sub>2</sub>, CH<sub>3</sub> etc., and torsion modes assigned out-of plane bending of C–H, C–C and some special modes for the title molecule. Because of the low symmetry of the studied molecule, mixed modes of the ring and also between the ring and

substituent, especially in the fingerprint region, are seen. The most difficult assignments are in-plane and out-of-plane modes, due to mixing with the ring and substituent modes.

#### 4.2.1. CH stretching vibrations

The C–H stretching vibrations appear in the region 3000–3100 cm<sup>-1</sup> for hetero aromatic structure, which is the characteristic region [43]. The C–H stretching bands appear generally in the 3000–3100 cm<sup>-1</sup> range in aromatic compounds, and the C–H in-plane and out-of-plane bending vibrations appear in the range of 1275–1000 cm<sup>-1</sup> and 900–690 cm<sup>-1</sup>, respectively [44]. The ring C–H stretching vibration modes of the title molecule are predicted at 3063 and 3081 cm<sup>-1</sup> by the B3LYP/6-311++G(d,p) method and observed at 3065 and 3095 cm<sup>-1</sup> in FT-IR and 3053 cm<sup>-1</sup> in FT-Raman, respectively. From the PED of the present molecule, these modes ( $\nu_1$ – $\nu_3$ ) involve approximately 100% contribution suggesting that they are pure stretching modes. The corresponding stretching modes are C<sub>1</sub>–H<sub>6</sub>, C<sub>3</sub>–H<sub>5</sub> and C<sub>18</sub>–H<sub>19</sub> units.

The frequencies of C–H ring vibrations are found higher than CH<sub>2</sub> and CH<sub>3</sub> groups. Methyl group (CH<sub>3</sub>) vibrations are generally referred to as electron-donating substituent in the aromatic rings system, the asymmetric C–H stretching (CH<sub>3</sub>) is expected around 2980 cm<sup>-1</sup> and the symmetric of them are observed at around 2870 cm<sup>-1</sup> [45–48]. The modes are separated always as symmetric and asymmetric. The symmetric modes have higher frequency than asymmetric ones for the ring, just the opposite for the CH<sub>2</sub> and CH<sub>3</sub> groups. The CH<sub>3</sub> and CH<sub>2</sub> modes are indicated in Table 3. These modes are seen in the literature; the band observed at 2952 cm<sup>-1</sup> (FT-IR) was assigned to CH<sub>3</sub> symmetric stretching and 2954 and 2961 cm<sup>-1</sup> were predicted for CH<sub>3</sub> symmetric stretching and 3016, 3001, 2995, and 2983 cm<sup>-1</sup> for CH<sub>3</sub> asymmetric modes (theoretically) for 4'-methylpropiofenone molecule [49]. The medium strong band was observed at 2941 cm<sup>-1</sup> in FT-Raman (symmetric) and predicted theoretically at 2978 and 2940 cm<sup>-1</sup> asymmetric and symmetric vibrations of CH<sub>2</sub> by B3LYP/6-311++G(d,p) level [49]. For 2,5-lutidine, the modes were observed at

**Table 3**  
Comparison of the calculated harmonic frequencies and experimental (FT-IR, FT-Raman and dispersive Raman) wavenumbers ( $\text{cm}^{-1}$ ) for S1 isomer of E-6-CLIN.

Modes no.	Sym.	Theoretical		Experimental			PED <sup>a</sup> ( $\geq 10\%$ )
		Unscaled freq.	Scaled freq.	FT-IR	FT-Raman	Dispersive Raman	
$\nu_1$	A'	3216	3081	3095			$\nu\text{CH}_{\text{sym.}}(\text{ring})$ (99)
$\nu_2$	A'	3198	3063	3065	3053	3070	$\nu\text{CH}_{\text{asym.}}(\text{ring})$ (100)
$\nu_3$	A'	3197	3063				$\nu\text{CH}_{\text{asym.}}(\text{ring})$ (99)
$\nu_4$	A''	3117	2986	2983	2998		$\nu\text{CH}_{\text{asym.}}(\text{CH}_2 \text{ and } \text{CH}_3)$ (99)
$\nu_5$	A'	3105	2974		2971	2973	$\nu\text{CH}_{\text{asym.}}(\text{CH}_2 \text{ and } \text{CH}_3)$ (100)
$\nu_6$	A''	3091	2961	2938		2939	$\nu\text{CH}_{\text{asym.}}(\text{CH}_2 \text{ and } \text{CH}_3)$ (99)
$\nu_7$	A'	3056	2927	2908	2902		$\nu\text{CH}_{\text{sym.}}(\text{CH}_2 \text{ and } \text{CH}_3)$ (99)
$\nu_8$	A'	3038	2910	2875	2850	2878	$\nu\text{CH}_{\text{sym.}}(\text{CH}_3)$ (100)
$\nu_9$	A'	1766	1692	1724		1725	$\nu\text{C}=\text{O}$ (89)
$\nu_{10}$	A'	1623	1595	1590	1596	1592	$\nu\text{CC}$ (45), $\nu\text{CN}$ (18), $\delta\text{CCN}$ (19), $\delta\text{CCH}_{\text{ring}}$ (10)
$\nu_{11}$	A'	1595	1568	1564			$\nu\text{CC}$ (40), $\nu\text{CN}$ (20), $\delta\text{CCN}$ (21)
$\nu_{12}$	A'	1519	1493				$\rho\text{CH}_2$ (81), $\tau\text{COCH}$ (18)
$\nu_{13}$	A'	1498	1473				$\rho\text{CH}_2$ (74), $\tau\text{COCH}$ (11), $\tau\text{CCCN}$ (11)
$\nu_{14}$	A'	1489	1464				$\delta\text{CCH}_{\text{ring}}$ (31), $\delta\text{CNH}$ (26), $\nu\text{CC}$ (18), $\delta\text{CCN}$ (12), $\nu\text{CN}$ (10)
$\nu_{15}$	A''	1487	1462	1457	1442	1450	$\rho\text{CH}_3$ (77), $\tau\text{COCH}$ (22)
$\nu_{16}$	A'	1429	1404		1412		$\omega\text{CH}_3$ (52), $\tau\text{COCH}$ (32)
$\nu_{17}$	A'	1400	1376				$\omega\text{CH}_3$ (53), $\tau\text{COCH}$ (37)
$\nu_{18}$	A'	1393	1370	1371	1366	1368	$\nu\text{CC}$ (26), $\nu\text{CN}$ (24), $\delta\text{CCH}_{\text{ring}}$ (23), $\delta\text{CCN}$ (11)
$\nu_{19}$	A'	1312	1290	1291	1324	1291	$\delta\text{CNH}$ (50), $\nu\text{CC}$ (18), $\delta\text{CCH}_{\text{ring}}$ (10), $\nu\text{CN}$ (10)
$\nu_{20}$	A'	1308	1286			1287	$\nu\text{CN}$ (40), $\nu\text{CC}$ (25), $\delta\text{CCH}_{\text{ring}}$ (14)
$\nu_{21}$	A''	1297	1276	1273			$\varphi\text{CH}_2$ [ $\delta\text{CCH}$ (67), $\tau\text{COCH}$ (24)]
$\nu_{22}$	A'	1282	1260				$\nu\text{CC}$ (54), $\nu\text{CO}$ (16), $\nu\text{CN}$ (11)
$\nu_{23}$	A''	1176	1156	1175	1190		$r\text{CH}_2$ [ $\text{CCH}$ (67), $\tau\text{COCH}$ (24)]
$\nu_{24}$	A'	1153	1133		1148		$\delta\text{CCH}_{\text{ring}}$ (51), $\nu\text{CC}$ (20), $\nu\text{CO}$ (10),
$\nu_{25}$	A'	1146	1127	1125			$\nu\text{CO}$ (31), $\nu\text{CC}$ (19), $\delta\text{CCH}_{\text{ring}}$ (19), $\delta\text{CCN}$ (10)
$\nu_{26}$	A'	1131	1112			1105	$\nu\text{CC}$ (15), $r\text{CH}_3$ (12), $\nu\text{CO}$ (10)
$\nu_{27}$	A'	1117	1099		1092		ring breath [ $\nu\text{CN}$ (30), $\nu\text{CC}$ (24), $\nu\text{CCL}$ (13)], $\delta\text{CCH}_{\text{ring}}$ (16)
$\nu_{28}$	A'	1039	1021	1023	1024	1023	ring def. [ $\delta\text{CCC}$ (27), $\nu\text{CC}$ (21), $\delta\text{CCN}$ (21)], $\nu\text{CO}$ (16)
$\nu_{29}$	A'	1031	1013				$\nu\text{CC}$ (38), $\nu\text{CO}$ (20), $\delta\text{CCN}$ (11), $\tau\text{COCH}$ (10), $\delta\text{CCC}$ (10)
$\nu_{30}$	A''	1011	994	994	994		$\gamma\text{CH}$ [ $\tau\text{CNCH}$ (80)], $\tau\text{CCCN}$ (16)
$\nu_{31}$	A''	969	954	952			$\gamma\text{CH}$ [ $\tau\text{CNCH}$ (81)], $\tau\text{CCCN}$ (10)
$\nu_{32}$	A'	886	871		896		$\nu\text{CO}$ (38), $\nu\text{CC}$ (18), $r\text{CH}_3$ [ $\tau\text{COCH}$ (18)]
$\nu_{33}$	A'	868	854	854		855	$\delta\text{CO}_2$ (21), $\nu\text{CO}$ (20), $\nu\text{CC}$ (15), $\delta\text{CCO}$ (13)
$\nu_{34}$	A''	863	848		837		$\gamma\text{CH}$ [ $\tau\text{CNCH}$ (78)]
$\nu_{35}$	A''	814	801	794	790	791	$r\text{CH}_3$ [ $\tau\text{COCH}$ (75), $r\text{CH}_2$ (12)]
$\nu_{36}$	A''	782	769	768			$\tau\text{CCCO}$ (44) + $\gamma\text{CH}$ [ $\tau\text{CNCH}$ (17)], $\tau\text{CCCN}$ (13)
$\nu_{37}$	A'	760	747	746	750	745	$\delta\text{CCN}$ (33), $\delta\text{CO}_2$ (18), $\nu\text{CCL}$ (14), $\nu\text{CC}$ (11)
$\nu_{38}$	A''	730	718	718			$\tau\text{CCCN}$ (50), $\tau\text{CCOO}$ (25), $\gamma\text{CH}$ (10)
$\nu_{39}$	A'	642	631	630	616	631	ring def. [ $\nu\text{CC}$ (11), $\delta\text{CCN}$ (54), $\delta\text{CCC}$ (23)]
$\nu_{40}$	A'	527	518	523	530		$\nu\text{CCL}$ (29), $\nu\text{CC}$ (29), $\delta\text{CCO}$ (25)
$\nu_{41}$	A''	494	486	488	487		$\tau\text{CCCN}$ (41), $\tau\text{CNCCI}$ (38)
$\nu_{42}$	A'	481	473				$\delta\text{CCO}$ (37), $\nu\text{CCL}$ (20), $\delta\text{CCN}$ (15), $\delta\text{CCC}$ (12)
$\nu_{43}$	A''	420	413	410	397	409	$\gamma\text{CH}$ [ $\tau\text{CCCN}$ (73), $\tau\text{CCCN}$ (23)]
$\nu_{44}$	A'	372	366			378	$r\text{CH}_3$ [ $\delta\text{CCO}$ (56), $\delta\text{CO}_2$ (22)]
$\nu_{45}$	A'	335	329				$\delta\text{NCCI}$ (52), $\delta\text{CCC}$ (15), $\delta\text{CCO}$ (13)
$\nu_{46}$	A''	291	286			285	$\varphi\text{CH}_3$ (31), $\tau\text{CNCCI}$ (17), $\tau\text{CCCN}$ (16)
$\nu_{47}$	A'	282	277				$\delta\text{CCN}$ (32), $\nu\text{CC}$ (24), $\delta\text{CCO}$ (21), $\nu\text{CCL}$ (12)
$\nu_{48}$	A''	250	246				$\varphi\text{CH}_3$ [ $\tau\text{COCH}$ (66)], $\tau\text{CCCC}$ (14)
$\nu_{49}$	A'	224	221		218		$\delta\text{CCO}$ (36), $\delta\text{CCC}$ (25), $\delta\text{NCCI}$ (21)
$\nu_{50}$	A''	131	129			120	$\tau\text{CCCO}$ (64), $\tau\text{CCCN}$ (20)
$\nu_{51}$	A'	91	90				$\delta\text{CCO}$ (60), $\delta\text{CCC}$ (28)
$\nu_{52}$	A''	74	73				$\tau\text{CCCO}$ (76), $\tau\text{CCCN}$ (11)
$\nu_{53}$	A''	67	66				$\tau\text{CCCN}$ (38), $\tau\text{CCCO}$ (25), $\tau\text{CCCC}$ (21), $\tau\text{COCH}$ (10)
$\nu_{54}$	A''	37	37				$\tau\text{CCCO}$ (88)

<sup>a</sup>  $\nu$ : stretching,  $\gamma$ : out-of plane bending,  $\delta$ : in-plane-bending,  $\tau$ : torsion,  $\rho$ : scissoring,  $\varphi$ : twisting,  $r$ : rocking,  $\omega$ : umbrella.

2980, 2959, 2935 and 2910  $\text{cm}^{-1}$  (FT-IR,  $\text{CH}_3$  asymmetric) and at 2875 and 2870  $\text{cm}^{-1}$  (in FT-Raman,  $\text{CH}_3$  symmetric) and  $\text{CH}_3$  stretching modes were assigned theoretically and were in good agreement with the experimental values [50]. The weak intensity peak at 2900  $\text{cm}^{-1}$  in (both of FT-IR and FT-Raman) was assigned to  $\text{CH}_3$  symmetric stretching mode, whereas  $\text{CH}_3$  asymmetric modes were predicted at 3020  $\text{cm}^{-1}$  and 2990  $\text{cm}^{-1}$  in FT-IR and as strong peaks were at 2940 and 2980  $\text{cm}^{-1}$  in FT-Raman due to  $\text{CH}_2$  symmetric and asymmetric stretching modes, respectively, for nicotinic acid ethyl ester molecule [40]. In this study, asymmetric CH modes are observed at 2983 and 2938  $\text{cm}^{-1}$  in FT-IR, at 2998 and 2971  $\text{cm}^{-1}$  in FT-Raman and 2973 and 2938  $\text{cm}^{-1}$  in dispersive Raman spectra for methyl and methylene groups. Also symmetric CH modes of  $\text{CH}_2$  and  $\text{CH}_3$  groups are observed at 2908 and 2875  $\text{cm}^{-1}$  in FT-IR, at 2902 and 2850  $\text{cm}^{-1}$  in FT-Raman

and at 2878  $\text{cm}^{-1}$  in dispersive Raman spectra. These modes are pure stretching. Their PEDs are ca. 100%. The corresponding methyl and methylene stretching modes are  $\text{C}_{14}\text{—H}_{15}$ ,  $\text{C}_{14}\text{—H}_{16}$ ,  $\text{C}_{14}\text{—H}_{17}$  ( $\text{CH}_3$ ) and  $\text{C}_{11}\text{—H}_{12}$ ,  $\text{C}_{11}\text{—H}_{13}$  ( $\text{CH}_2$ ) units. If we consider the literature and experimental results mentioned, the predicted values have good coherence with their related values.

#### 4.2.2. CC vibration modes

The C—C (carbon-carbon) stretching vibrations in ring are very much important and highly characteristic. The bands are of variable intensity and observed at 1625–1590, 1575–1590, 1470–1540, 1430–1465, and 1280–1380  $\text{cm}^{-1}$  from the frequency ranges given by Varsányi [51]. In the aromatic six membered rings, e.g. benzene and pyridines, there are two or three bands, due to skeletal vibrations, the

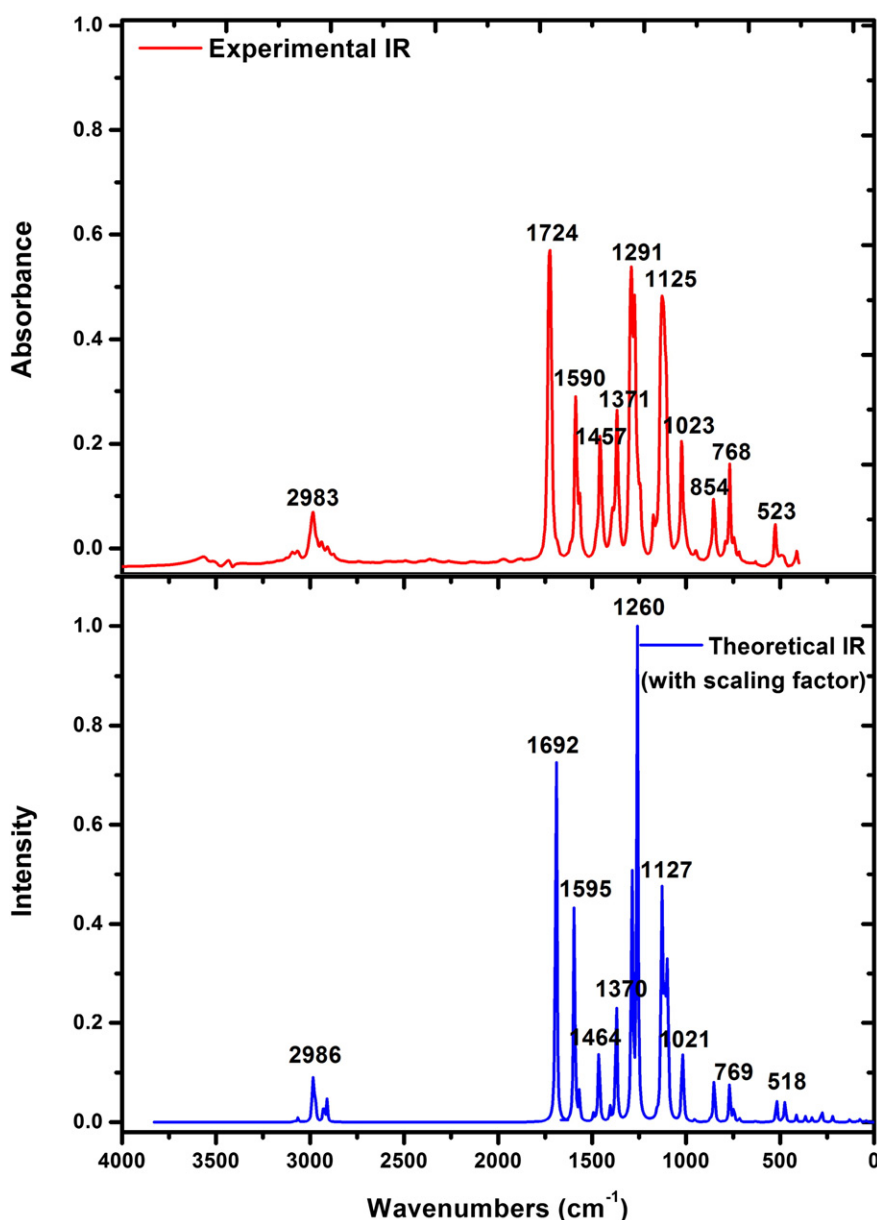


Fig. 2. The calculated (with the scale factor) and experimental FT-IR spectra of E-6-CIN.

strongest usually being at about  $1500\text{ cm}^{-1}$  [50]. The C—C modes were predicted at  $1578$  and  $1581\text{ cm}^{-1}$  (using B3LYP and B3PW91) and are in excellent agreement with experimental observations of  $1581\text{ cm}^{-1}$  in FT-IR spectrum for 2-chloronicotinic acid molecule [34]. Govindarajan et al. [50] observed very strong intensities at  $1610$ ,  $1570$ ,  $1490$ , and  $1480\text{ cm}^{-1}$  and predicted theoretically the CC stretching vibrations at  $1612$ ,  $1576$ ,  $1493$ , and  $1475\text{ cm}^{-1}$ . The aromatic ring carbon–carbon stretching vibrations occur in the region of  $1430$ – $1625\text{ cm}^{-1}$  and the strong C—C aromatic stretch was observed in the region of  $1250$ – $1550\text{ cm}^{-1}$  in FT-IR spectrum, calculated in the range of  $1277$ – $1554\text{ cm}^{-1}$  [52]. In this study, two strong C—C modes near the  $1500\text{ cm}^{-1}$  were assigned at  $1568$  and  $1595\text{ cm}^{-1}$  by using B3LYP method and observed at  $1564$  and  $1590$  (FT-IR),  $1596$  (FT-Raman) and  $1592\text{ cm}^{-1}$  (dispersive Raman), respectively. The highest contribution mode of C—C vibrations is seen at  $1260\text{ cm}^{-1}$  (missed in experiment) in the present work. The theoretical values of C—C stretching modes are in very good coherence with their experimental data.

However the C—C stretching modes generally mixed other ring modes showing to their PED.

#### 4.2.3. C—N vibration modes

The C—N vibration is a very difficult assignment, due to the overlapping of the other vibrations in the pyridine ring; however these bands were recorded at  $1030$ – $1600\text{ cm}^{-1}$  in FT-IR and  $1030$ – $1590\text{ cm}^{-1}$  in FT-Raman, respectively [40]. Sundaraganesan et al. [53] calculated C—N stretching at  $1381\text{ cm}^{-1}$ . Karabacak et al. [54] assigned the modes at  $1272$  and  $1258\text{ cm}^{-1}$  in FT-IR spectrum and predicted at  $1264$  and  $1274\text{ cm}^{-1}$  for 2/6-bromonicotinic acid, respectively. The C—N band was observed at  $1374\text{ cm}^{-1}$  in FT-IR spectrum ( $1376\text{ cm}^{-1}$  in FT-Raman) and calculated theoretically at  $1371\text{ cm}^{-1}$  mixing other vibrations [35]. In the present work, the C—N stretching vibrations are predicted at  $1286$  and  $1370\text{ cm}^{-1}$  and their PED contributes 40 and 24%. The observed values are at  $1371\text{ cm}^{-1}$  (FT-IR),  $1287$

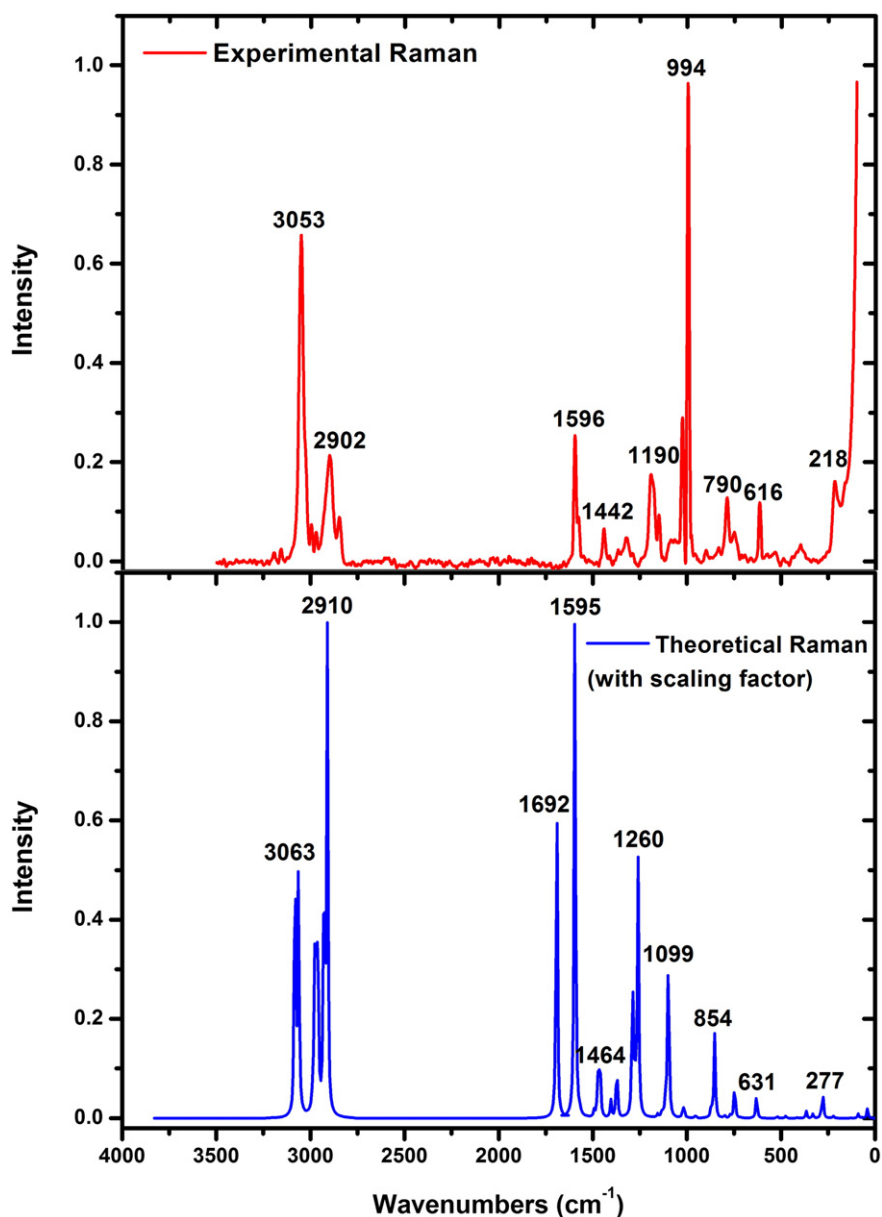


Fig. 3. The calculated (with the scale factor) and experimental FT-Raman spectra of E-6-CIN.

and  $1366\text{ cm}^{-1}$  (FT-Raman) and  $1368\text{ cm}^{-1}$  (dispersive Raman), respectively, shown in Table 3.

#### 4.2.4. CCl vibration modes

Mooney [55] assigned vibrations of C—X group (X = Cl, Br, I) in the frequency range of  $1129\text{--}480\text{ cm}^{-1}$ . For 4-chloro-2-fluoroaniline molecule, the band was found at  $858\text{ cm}^{-1}$  in FT-IR spectrum (C—Cl stretching 78% TED), at  $575\text{ cm}^{-1}$  in IR and Raman (C—Cl in-plane), and at  $323\text{ cm}^{-1}$  in Raman (C—Cl out-of-plane deformation), respectively [56]. Arivazhagan et al. [57] observed the C—Cl stretching bands at  $670$  and  $680\text{ cm}^{-1}$  (FT-IR and FT-Raman). As shown in Table 3, the C—Cl vibrations are assigned various mixed stretching modes calculated at  $747$ ,  $518$ , and  $473\text{ cm}^{-1}$ . The C—Cl stretching modes are observed at  $746$  and  $523\text{ cm}^{-1}$  (FT-IR), at  $750$  and  $530\text{ cm}^{-1}$  (FT-Raman) and at  $745\text{ cm}^{-1}$  (dispersive Raman), respectively, for the present paper. These results are agree well with their experiment and in the literature [50–52].

#### 4.2.5. C=O and C—O vibration modes

The C=O bond was formed by  $\pi\text{--}\pi$  between C and O; internal hydrogen bonding reduces the frequencies of the C=O stretching absorption to a greater degree than intermolecular H bonding because of the different electronegativities of C and O, and the bonding is not equally distributed between the two atoms [40]. The C=O modes are observed in the region  $1700\text{--}1800\text{ cm}^{-1}$  [40,58–60]. The band of C=O stretching was observed at  $1725\text{ cm}^{-1}$  in Raman spectrum by Sala et al. [61]. The sharp intense band in infrared spectrum at  $1679\text{ cm}^{-1}$  was assigned to C=O stretching mode, observed in Raman spectrum at  $1680\text{ cm}^{-1}$  as a strong band for ethyl p-amino benzoate molecule [39]. The C=O bands were recorded at  $1724\text{ cm}^{-1}$  and  $1725\text{ cm}^{-1}$  FT-IR and dispersive Raman, respectively, and predicted at  $1692\text{ cm}^{-1}$  (scaled). The PED value is 89% for E-6-CIN molecule as reported in Table 3. The strongest band of C=O stretching mode appeared in the experimental FT-IR spectrum whereas decreased intensity in dispersive Raman spectrum and missed in FT-Raman (see Figs. 2–4).

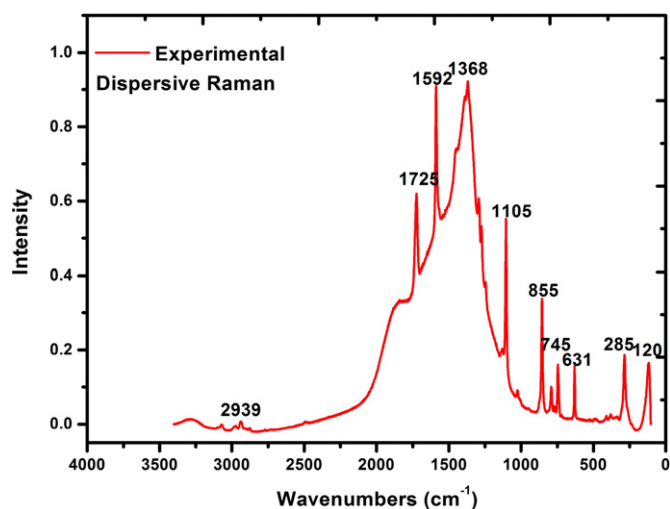


Fig. 4. Dispersive Raman spectrum of E-6-CIN.

#### 4.2.6. Bending and torsion vibration modes

The in-plane and out-of-plane bending of C—H vibrations generally appears in the range of 1000–1300  $\text{cm}^{-1}$  and 750–1000  $\text{cm}^{-1}$ , respectively, for aromatic compounds [43,47]. Kose et al. [42] observed the C—H in-plane bending modes between 1143 and 1312  $\text{cm}^{-1}$  in FT-Raman and observed the C—H out-of-plane bending vibrations at 994 and 911  $\text{cm}^{-1}$  in FT-Raman for dinicotinic acid molecule. In this study, the C—H bending modes were recorded at 1099, 1127, 1133, 1286, 1290, 1370, and 1464  $\text{cm}^{-1}$  as in-plane bending and 848, 954, and 994  $\text{cm}^{-1}$  as out-of plane bending and showed good correlation with their experimental results (especially at 1291, 1371, 1125, and 952  $\text{cm}^{-1}$  FT-IR; 1366, 1287, and 994  $\text{cm}^{-1}$  FT-Raman; and 1368  $\text{cm}^{-1}$  dispersive Raman). The PED contributions of out-of plane modes show to be purer than in-plane modes. Namely, the in-plane bending vibrations are mixed with other bending modes for E-6-CIN molecule. The bands at 1099  $\text{cm}^{-1}$  (1092  $\text{cm}^{-1}$  FT-Raman) were assigned the ring breathing mode. Our results show good coefficient with their experiment and the literature for the similar molecules [32,34,39,40].

The CH bending vibrations of the ethyl group are classified as scissoring, umbrella, twisting, and rocking modes. The scissoring mode was characterized by the strong IR band at 1475  $\text{cm}^{-1}$  and was computed at 1475  $\text{cm}^{-1}$  for methylene group [39]. The most important of the rocking and scissoring vibrational modes were mixed modes of  $\text{CH}_2$  and  $\text{CH}_3$  viz., the bands at 1370  $\text{cm}^{-1}$  (both), 1330  $\text{cm}^{-1}$  (FT-IR) and 790  $\text{cm}^{-1}$  (both) were assigned to rocking modes whereas medium peaks at 1450  $\text{cm}^{-1}$  and 1480  $\text{cm}^{-1}$  (FT-IR) to scissoring modes [40]. In this study, for E-6-CIN molecule, the scissoring modes of methyl and methylene groups are calculated at 1462, 1473, and 1493  $\text{cm}^{-1}$  and recorded at 1457, 1442, and 1450  $\text{cm}^{-1}$  in FT-IR, FT-Raman and dispersive Raman, respectively. Cinar et al. [62] observed at 1507, 1449 and 1400  $\text{cm}^{-1}$  in FT-IR and 1515, 1451 and 1403  $\text{cm}^{-1}$  in FT-Raman as an umbrella modes of  $\text{CH}_3$ . In accordance to this we calculated at 1404 and 1376  $\text{cm}^{-1}$  as an umbrella and missed the experimental results (except 1412  $\text{cm}^{-1}$  in FT-Raman). The rocking vibrations usually appear within the region 1070–1010  $\text{cm}^{-1}$  [50,63,64]. The strong peak at 1170  $\text{cm}^{-1}$  (FT-IR) was assigned to rocking vibration of  $\text{CH}_2$  [40] and the recorded at 1045 and 1038  $\text{cm}^{-1}$  is assigned to out-of-plane  $\text{CH}_3$  rocking vibrations [50]. The band at 1005  $\text{cm}^{-1}$  in FT-IR and 988  $\text{cm}^{-1}$  in Raman ( $\text{CH}_2$ ) and the band at 1154  $\text{cm}^{-1}$  in Raman ( $\text{CH}_3$ ) were assigned to rocking in-plane vibration for 4-aminobenzoate molecule [65]. The out-of-plane rocking modes ( $\text{CH}_3$ ) were observed around 1129  $\text{cm}^{-1}$  in FT-Raman spectrum for 4-aminobenzoate molecule [65]. With reference to literature data, the rocking modes of the title molecule are found

at 1156  $\text{cm}^{-1}$  ( $\text{CH}_2$ ) and 1112, 871, 801 and 366  $\text{cm}^{-1}$  ( $\text{CH}_3$ ). They are in good agreement with their experimental values.

For nicotinic acid ethyl ester molecule, the O=C=O and C—C—O bending vibrations were assigned a strong band in Raman spectrum (850  $\text{cm}^{-1}$ ) and a weak band at 390  $\text{cm}^{-1}$ , respectively [40]. In the present work the bands 90, 221, 277, 329, 473, 518, and 854  $\text{cm}^{-1}$  are calculated and assigned C—C—O in-plane bending vibrations and observed at 523 and 854  $\text{cm}^{-1}$  (FT-IR), 218  $\text{cm}^{-1}$  (FT-Raman) and 855  $\text{cm}^{-1}$  (dispersive Raman). The  $\text{CO}_2$  vibrations are calculated at 366, 747 and 854  $\text{cm}^{-1}$  and observed at 746/854  $\text{cm}^{-1}$  in FT-IR, 750  $\text{cm}^{-1}$  in FT-Raman, and 378/745/855  $\text{cm}^{-1}$  in dispersive Raman, respectively.

The assigned in-plane bending modes of CN ( $\delta\text{CN}$  or  $\delta\text{CNC}$  or  $\delta\text{NCC}$ ) are separated broad band 1595, 1568, 1021, 747, 631, 473, and 277  $\text{cm}^{-1}$  and in good agreement with the experimental data. The highest contribution comes from modes  $\nu_{37}$  and  $\nu_{47}$ . These modes are generally mixed with the other bending modes. CNC in-plane bending mode (for similar molecule) was recorded at 620  $\text{cm}^{-1}$  medium and strong intensity in FT-IR and FT-Raman, respectively [40].

The torsion and out-of-plane bending modes of ring and other groups for E-6-CIN molecule are obtained in a wide band like vibrational modes of the studied molecule. Therefore, these modes will not be discussed here. Also the PEDs of these modes can be seen from the last columns of Table 3.

#### 4.2.7. Analysis of vibrational calculations

The graphics of correlation between the experimental and calculated wavenumbers are plotted. FT-IR, FT-Raman and dispersive Raman correlation graphics were given in Figs. S2 (a–c). As seen from figures, the experimental wavenumbers have a better correlation and the relations between the experimental and calculated wavenumbers are usually linear and described for infrared, Raman, and dispersive Raman spectra, respectively by the next equations:

$$\begin{aligned} v_{\text{cal}} &= 1.0042 v_{\text{exp}} - 4.8879 & (R^2 &= 0.9998 \text{ for Infrared}) \\ v_{\text{cal}} &= 1.0068 v_{\text{exp}} - 7.8648 & (R^2 &= 0.9996 \text{ for Raman}) \\ v_{\text{cal}} &= 1.0033 v_{\text{exp}} - 2.0261 & (R^2 &= 0.9998 \text{ for dispersive Raman}) \end{aligned}$$

#### 4.2.8. NMR spectra

Nuclear magnetic resonance was explained through the experimental observations and the molecular quantum chemistry DFT calculations. To have the calculations of NMR, firstly, the full geometry optimization was performed and the gradient corrected density functional level of theory using the hybrid B3LYP method based on Becke's three parameters functional of DFT and gauge-including atomic orbital

Table 4

Experimental and theoretical,  $^1\text{H}$  and  $^{13}\text{C}$  NMR chemical shifts (with respect to TMS) of E-6-CIN with DFT (B3LYP/6-311++G(d,p)) method.

Atoms	Exp.	B3LYP
C(1)	140.80	146.48
C(2)	125.92	130.41
C(3)	151.19	156.16
C(4)	155.04	168.79
C(8)	164.50	171.43
C(11)	62.09	66.17
C(14)	14.65	13.69
C(18)	125.26	129.31
H(5)	8.85	9.13
H(6)	8.26	8.58
H(12)	4.32	4.25
H(13)	4.32	4.25
H(15)	1.31	1.35
H(16)	1.31	1.50
H(17)	1.31	1.50
H(19)	7.64	7.61



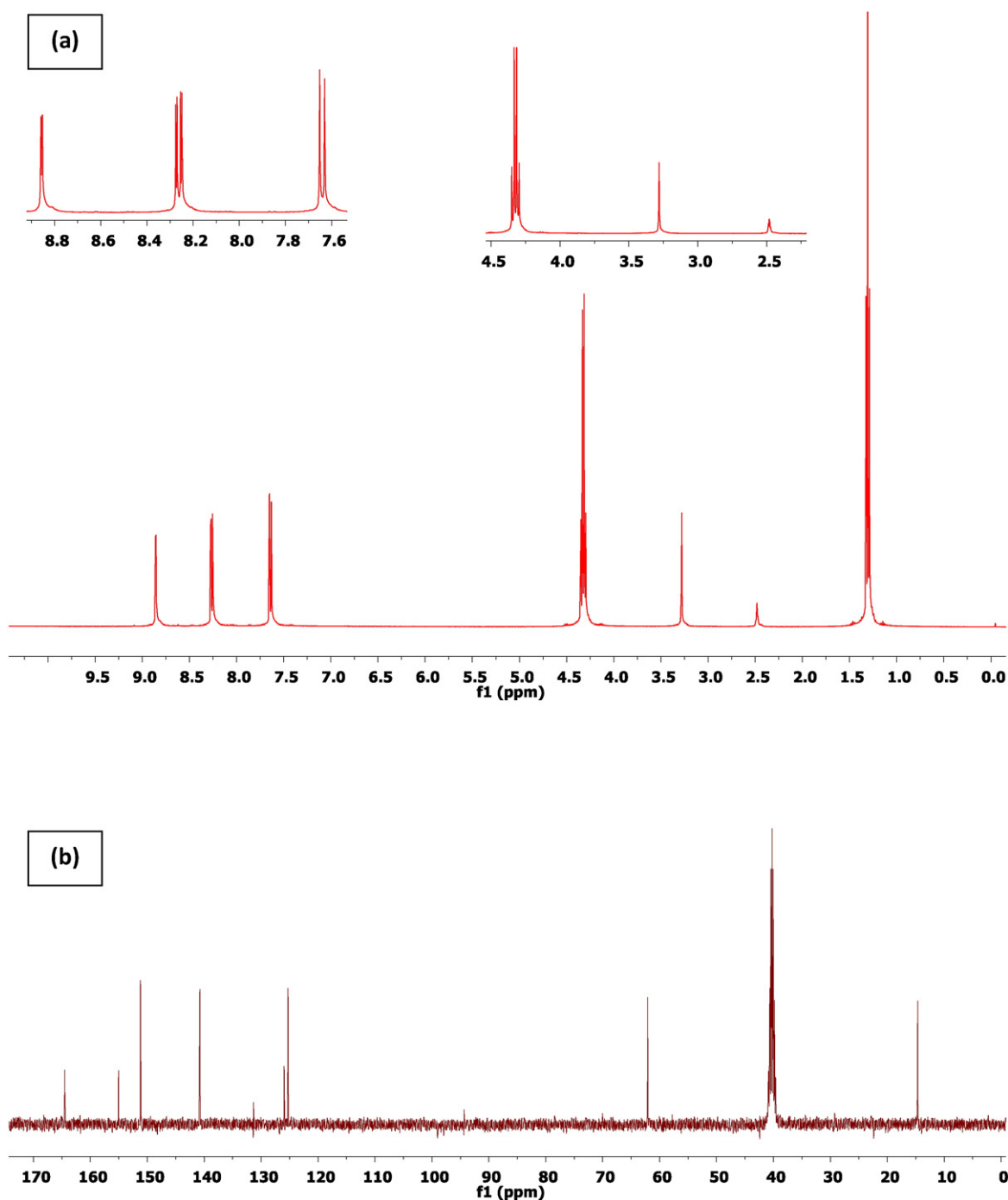


Fig. 5. (a) <sup>1</sup>H NMR; (b) <sup>13</sup>C NMR spectra of E-6-CIN in DMSO solution.

(GIAO) [18,19] for the 6-311++G(d,p) basis set in DMSO solution. To have accurate predictions of the molecular geometries is essential for reliable calculations of magnetic properties. The isotropic shielding values were used to calculate the isotropic chemical shifts  $\delta$  with respect to tetramethylsilane (TMS)  $\delta_{iso}^X = \sigma_{iso}^{TMS} - \sigma_{iso}^X$ .

The experimental and theoretical <sup>1</sup>H and <sup>13</sup>C chemical shifts in DMSO solution solvent are collected in Table 4. The atoms were numbered according to Fig. 1. The experimental <sup>1</sup>H and <sup>13</sup>C NMR spectra of the studied molecule are shown in Fig. 5. The proton chemical shifts of organic molecules generally vary greatly with the electronic environment of the proton. Hydrogen attached or nearby electron-donating atom or group increases the shielding and moves the resonance towards a lower frequency, whereas electron-withdrawing atom or group can decrease the

shielding and move the resonance of attached proton towards a higher frequency [66].

The NMR chemical shifts of aromatic protons of organic molecules are usually observed in the range of 7.00–8.00 ppm. In this paper, the signals of proton (<sup>1</sup>H) NMR of E-6-CIN molecule were experimentally observed in the range of 7.64–8.85 ppm and theoretically calculated in the range of 7.61–9.13 ppm for the aromatic protons of ring. The H5 value is computed bigger than the other proton chemical shifts due to the electronic environment of H5 atom. Also the chemical shift of H19 atom was observed as smaller one in the ring; this may be due to the chlorine atoms and/or DMSO solvent effects. However the chemical shifts of hydrogen atoms of methylene and methyl groups were recorded as 4.32 and 1.31 ppm, respectively. Due to the methyl protons

**Table 5**

Experimental and calculated wavelengths  $\lambda$  (nm), excitation energies (eV), oscillator strengths ( $f$ ) of E-6-CIN gas phase, in ethanol and DMSO solution.

$\lambda$ (nm)	$E$ (eV)	$f$	Major contributors
<i>Gas</i>			
274.23	4.5217	0.0005	H-1 $\rightarrow$ L (97%)
248.15	4.9971	0.0001	H-2 $\rightarrow$ L (92%)
245.18	5.0576	0.0028	H-1 $\rightarrow$ L + 1 (90%)
<i>Ethanol</i>			
266.67	4.6499	0.0006	H-1 $\rightarrow$ L (97%)
249.79	4.9642	0.3252	H $\rightarrow$ L (76%), H $\rightarrow$ L + 1 (13%)
243.36	5.0953	0.0000	H-2 $\rightarrow$ L (95%)
<i>DMSO</i>			
266.40	4.65463	0.0006	H-1 $\rightarrow$ L (97%)
250.05	4.95897	0.3363	H $\rightarrow$ L (77%), H $\rightarrow$ L + 1 (12%)
243.19	5.09899	0.0000	H-2 $\rightarrow$ L (95%)

resonance at 1.31 ppm and the two equal neighboring protons, signal splits into triplets and also is quite low. The electron withdrawing ability of oxygen atoms decreases the electron density around protons, causing low field shift. All hydrogen atoms of methyl groups chemical shift values are  $S \leq 3$  ppm due to the shielding effect [50]. The methylene protons bounded to oxygen atom of the studied molecule have resonance at 4.32 ppm. Cinar and Karabacak obtained this state for structurally similar molecule at 4.29 ppm as resonance [67].

The characteristic chemical shift of aromatic carbons gives signals in the region from 100 to 150 ppm in overlapped area [68,69]. The E-6-CIN molecule has eight (five + three) carbon atoms. The  $^{13}\text{C}$  NMR chemical shifts are evaluated as the state of carbons. The C1–C4, C18 and C8 are observed and calculated as bigger than the chemical shifts of C11

and C14 carbon atoms. In this study, low-field shift of carbonyl carbon (C8) is recorded in  $^{13}\text{C}$  NMR spectrum at 164.50 ppm in DMSO solution. A careful look at any  $^{13}\text{C}$  NMR spectrum having methyl and methylene signals will show that the peaks of  $\text{CH}_3$  carbons are similar in intensities or smaller than those of  $\text{CH}_2$  carbon atoms. The resonances of  $\text{CH}_2$  and  $\text{CH}_3$  group of the title molecule are observed at 62.09 and 14.65 ppm with similar intensity. The computed values were shown in the same parallel as seen in Table 4. The computed and recorded results are in very good agreement for the similar structures [50,67].

Based on the experimental results of  $^1\text{H}$  and  $^{13}\text{C}$  NMR chemical shifts of E-6-CIN molecule are described fairly well by the selected DFT method combined with the basis set. Also to see coherence between the experimental and theoretical total chemical shifts of the present molecule correlation graphics were plotted as Fig. S3. Also the correlation graphics of  $^1\text{H}$  and  $^{13}\text{C}$  NMR were presented as Figs. S4 and S5. The relations between the experimental chemical shifts ( $\delta_{\text{exp}}$ ) and the calculated ones were described by the following equations:

$$\begin{aligned} \text{Total : } \delta_{\text{cal}}(\text{ppm}) &= 1.0495\delta_{\text{exp}} - 0.2827 \quad (R^2 = 0.9993) \\ ^1\text{H : } \delta_{\text{cal}}(\text{ppm}) &= 1.0135\delta_{\text{exp}} + 0.0400 \quad (R^2 = 0.9978) \\ ^{13}\text{C : } \delta_{\text{cal}}(\text{ppm}) &= 1.0569\delta_{\text{exp}} - 1.3125 \quad (R^2 = 0.9974) \end{aligned}$$

### 4.3. Electronic properties

#### 4.3.1. Frontier molecular orbital analysis

It is obvious that to use TD-DFT calculations to predict the electronic absorption spectra is a quite reasonable method. Because of this, the

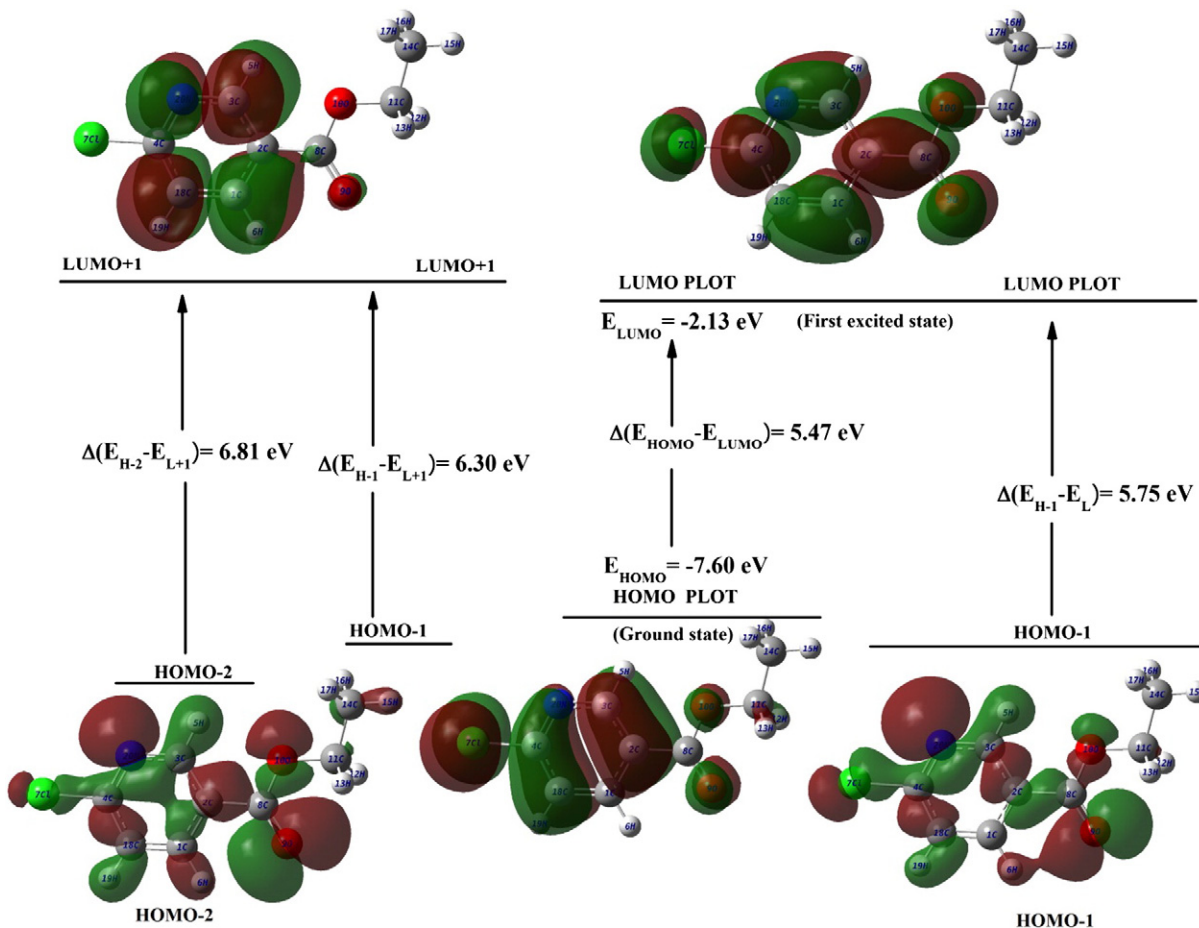


**Fig. 6.** The selected frontier molecular orbitals of E-6-CIN with the energy gaps.

**Table 6**  
The calculated energy values for S1 isomer of E-6-CIN molecule.

TD-DFT/B3LYP/6-311++G(d,p)	Gas	Ethanol	DMSO
$E_{\text{total}}$ (Hartree)	−975.25187752	−975.25995234	−975.26021629
$E_{\text{HOMO}}$ (eV)	−7.60	−7.64	−7.64
$E_{\text{LUMO}}$ (eV)	−2.13	−2.15	−2.15
$E_{\text{HOMO}−1}$ (eV)	−7.88	−8.04	−8.04
$E_{\text{HOMO}−2}$ (eV)	−8.39	−8.50	−8.50
$E_{\text{LUMO}+1}$ (eV)	−1.58	−1.56	−1.56
$E_{\text{HOMO}−\text{LUMO}}$ gap (eV)	5.47	5.49	5.49
$E_{\text{HOMO}−1−\text{LUMO}}$ gap (eV)	5.75	5.89	5.89
$E_{\text{HOMO}−1−\text{LUMO}+1}$ gap (eV)	6.30	6.48	6.48
$E_{\text{HOMO}−2−\text{LUMO}+1}$ gap (eV)	6.81	6.94	6.94
Chemical hardness ( $\eta$ )	2.74	2.75	2.75
Electronegativity ( $\chi$ )	4.87	4.90	4.90
Chemical potential ( $\mu$ )	−4.87	−4.90	−4.90
Electrophilicity index ( $\omega$ )	4.33	4.36	4.36

excitation energies, absorbance and oscillator strengths for the molecule after optimized geometry in the ground state are obtained in the framework of TD-DFT calculations with the B3LYP/6-311++G(d,p) method. The computed electronic values, such as absorption wavelengths ( $\lambda$ ), excitation energies ( $E$ ), and oscillator strengths ( $f$ ) are tabulated in Table 5. The contributions of transitions are calculated by using GaussSum 2.2 [28] and presented in Table 5 showing major contributions.

The frontier molecular orbitals, called highest occupied molecular orbital (HOMO) and lowest unoccupied molecular orbital (LUMO), are the most important orbitals in a molecule and very useful for physicists and chemists is the main orbital taking part in chemical reaction. The HOMO (H) energy characterizes the ability of electron giving; LUMO (L) energy characterizes the ability of electron accepting. The energy of the HOMO is directly related to the ionization potential, while LUMO energy is directly related to the electron affinity [70]. The conjugated molecules are characterized by a small highest occupied molecular orbital–lowest unoccupied molecular orbital (H–L) separation, which is the result of a significant degree of intra-molecular charge transfer from the end-capping electron-donor groups to the efficient electron-acceptor group [71].

The surfaces of some important FMOs (major contributions) are drawn and given in Fig. 6 to understand the bonding scheme of our studied molecule. The HOMO and LUMO energy are calculated as −7.60 eV and −2.13 eV for gas phase by TD-DFT method, respectively. The energy difference between  $H \rightarrow L$ ,  $H-1 \rightarrow L$ ,  $H-1 \rightarrow L+1$  and  $H-2 \rightarrow L+1$  orbital is a critical parameter in determining molecular electrical transport properties because it is a measure of electron conductivity. The most important energy gaps ( $H \rightarrow L$ ,  $H-1 \rightarrow L$ ,  $H-1 \rightarrow L+1$  and  $H-2 \rightarrow L+1$ ) are calculated 5.47, 5.75, 6.30 and 6.81 eV for gas phase of E-6-CIN molecule in Table 6. These values are calculated in two solvents (ethanol and DMSO) of the present molecule and given in Table 6.

The nodes, shown in red and green colors which are positive and negative phase, respectively, of molecular orbitals (H, L, L+1) are placed nearly symmetrically. However the H-1 and H-2 have no symmetrical nodes. The HOMO has a charge density localized over the ring of the entire molecule except  $\text{CH}_3$  group, but the LUMO is characterized by a charge distribution except  $\text{CH}_2$  and  $\text{CH}_3$  group. H-2, the negative (green) nodes, are located randomly. The energy gaps of the title molecule are given in Fig. 6 and Table 6. The energy gap explains the eventual charge transfer interactions taking place within the molecule.

Moreover the values of chemical hardness, electronegativity, chemical potential and electrophilicity are collected for the molecule in gas phase, ethanol and DMSO solutions in Table 6. These chemical quantities are obtained by use of HOMO and LUMO energies. They are good indicators of the chemical stability of molecular systems [56]. An index of reactivity measures the escaping tendency of electron cloud named as chemical hardness ( $\eta$ ) and potential ( $\mu$ ), respectively, given by Parr

and Pearson [72],  $\eta = (I - H)/2$  and  $\mu = -(I + H)/2$ . I and H are ionization potential and electron affinity of a molecular system. If the molecule has large energy gaps, it is a hard molecule; otherwise, if it has small energy gaps, it is a soft molecule. Hard molecules are less polarizable than the soft molecules because it needs big excitation energy. The other chemical quant is electronegativity ( $\chi$ ) is described as negative of the electronic chemical potential. Global electrophilicity index ( $\omega$ ), which is introduced by Parr et al. [73] and measures the stabilization energy, has been given by the following expression:  $\omega = \mu^2/2\eta$ , in terms of electronic chemical potential  $\mu$  and chemical hardness  $\eta$ , and assesses the lowering of energy due to maximal electron flow between donor and acceptor. In this paper, the chemical hardness  $\eta$  has the same magnitude for ethanol and DMSO solvents. The chemical potential and electrophilicity index are increased in the solvents.

#### 4.3.2. Total, partial, and overlap population density of states

The PDOS, TDOS, and OPDOS (COOP) density of states of E-6-CIN are plotted in Fig. 7 and Figs. S6 and S7, respectively, created by convoluting the molecular orbital information with Gaussian curves of unit height and Full width at half maximum (FWHM) of 0.3 eV using the GaussSum 2.2 program [28] to ensure a pictorial presentment of molecule orbital (MO) compositions and their contributions to chemical bonding.

Their contributions to chemical bonding through the OPDOS plots, which are also referred in the literature as COOP diagrams, show the bonding, anti-bonding and nonbonding nature of the interaction of the two orbitals, atoms or groups. Positive values of the OPDOS show a bonding interaction (because of the positive overlap population), negative values assign that there is an anti-bonding interaction (due

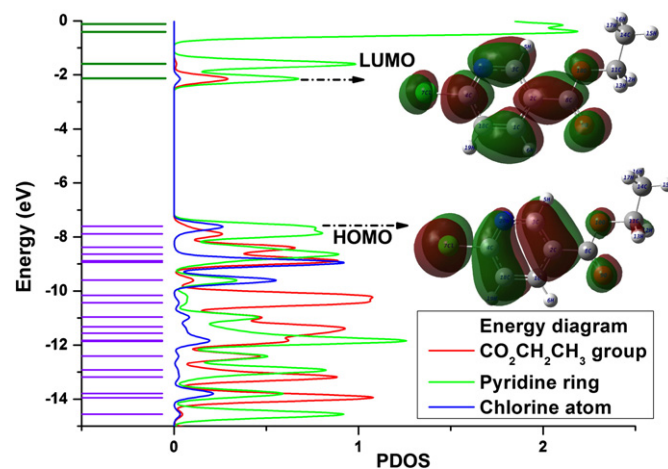


Fig. 7. The partial electronic density of states diagram of E-6-CIN.

to negative overlap population) and zero value indicates nonbonding interactions [74].

As seen in Fig. 6, the nodes of HOMO orbitals are settled on ring (68%) and chlorine atom (26%) and two oxygen atoms (3%), their total contributions ca. 100%. The LUMO orbitals are settled on the COOH (29%), ring (68%) and chlorine atom (3%) of the compound. Also Fig. S7 (the OPDOS diagram) has shown some of orbitals of energy values of interaction between selected groups which are shown from figures clearly: pyridine ring  $\leftrightarrow$  CO<sub>2</sub>CH<sub>2</sub>CH<sub>3</sub> groups (black line) CO<sub>2</sub>CH<sub>2</sub>CH<sub>3</sub>  $\leftrightarrow$  chlorine atom (red line) and pyridine ring  $\leftrightarrow$  chlorine atom (blue line).

#### 4.3.3. Molecular electrostatic potential surface

The molecular electrostatic potential surface (MEPs) is superimposed on top of the total energy density as a shell, due to usefulness of studying reactivity given that an approaching electrophile will be attracted to negative regions (where the electron distribution effect is dominant). The

maximum negative region which is preferred site for electrophilic attack is indicated by red color, while the maximum positive region which is preferred site for nucleophilic attack symptoms by blue color [75].

The MEPs of the studied molecule is plotted in 3D and 2D plots are illustrated in Fig. 8. The different values of the electrostatic potential at the surface are presented with different colors in the map of MEPs. Potential increases in the order of red to blue color. The range between  $-0.04266$  a.u. (dark red) and  $0.04266$  a.u. (dark blue) is aligned as a color code of the maps for the present molecule, where blue indicates the strongest attraction and red indicates the strongest repulsion. The MEPs of the molecule has shown that negative potential regions are localized near N20 and O9 atoms, respectively. The regions having the negative and the positive potential are over the electronegative atom (N20 and O9 atoms) and near the hydrogen atoms (especially H6 and H19 atoms), respectively.

The negative potential values are  $-0.0399379$  (N20 atom) and  $-0.0397748$  (O9 atom) a.u., while the positive potential values are

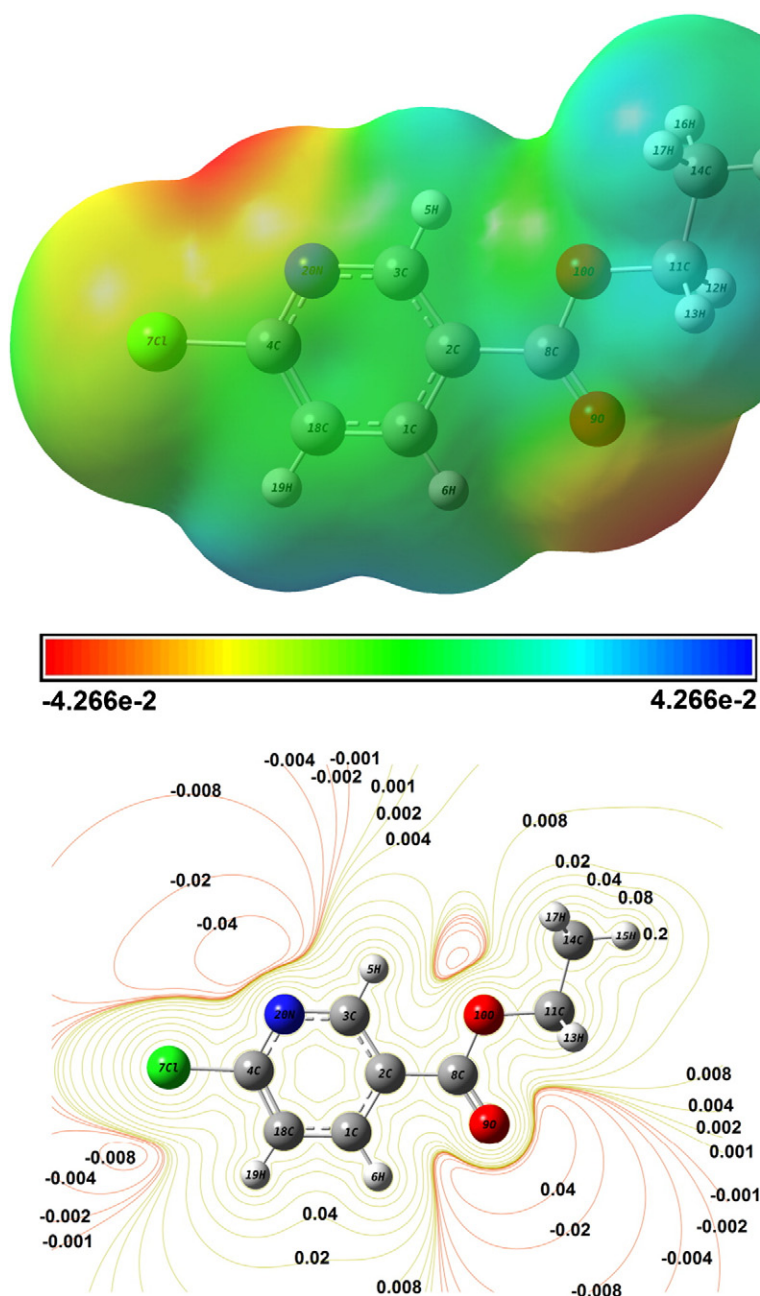


Fig. 8. The molecular electrostatic potential 3D contour map and 2D map for E-6-CIN molecule.

0.0278126 a.u. (H19 and H6 atoms) and 0.0220115 a.u. (CH<sub>3</sub> group), respectively. The N20 atom has nearly the same negative potential value with the O9 atom. However H19 and H6 atoms have higher positive potential value than CH<sub>3</sub> group. As a result, the H atoms indicate that the strongest attraction and N20 and O9 atom indicate the strongest repulsion.

#### 4.3.4. Mulliken atomic charges

The Mulliken atomic charges of the methyl 6-chloronicotinate (M-6-CIN) and E-6-CIN were given in Table S1 and shown in Fig. S8, computed by using the DFT/B3LYP method 6-311++G(d,p) basis set. To see the change of charges easily column chart is given in Fig. S9, because the calculation of reactive atomic charges play an important role in the application of quantum mechanical calculations in the molecular system. When adding the CH<sub>3</sub> group to methyl 6-chloronicotinate molecule, the Mulliken atomic charges showed different values. The charges of C11 atom are different distribution (negative or positive) for two molecules; however, the charges of the other atoms give the same charge with each other as seen in Figs. S8 and S9. Hydrogen atoms exhibit a positive charge, which is an acceptor atom for each one.

#### 4.4. Thermodynamic properties

The thermodynamic parameters (such as zero-point vibrational energy, thermal energy, specific heat capacity, rotational constants, entropy and dipole moment) of S1 and S2 isomers of the molecule are calculated by using DFT/B3LYP/6-311++G(d,p) method at room temperature (298.15 K) in the ground state. The global minimum energy is obtained for the stable structure S1 after optimized by B3LYP with 6-311++G(d,p) basis set as  $-975.25187752$  a.u. and the zero-point vibrational energies (ZPVEs) as  $93.79120$  kcal mol<sup>-1</sup> (Table S2). Also the same selected parameters of S2 isomer of E-6-CIN molecule are given in Table S2. Moreover, change of thermodynamic functions (heat capacity, entropy and enthalpy) is shown according to varying temperature for S1 isomer of E-6-CIN molecule, as scanning from 100 to 700 K, for every 50 K due to the fact that the molecular vibrational intensities increase with temperature. Table S3 showed the obtained thermodynamic functions based on varied temperature in accordance to vibrational analysis. These thermodynamic functions are increasing with temperature. The correlation equations between temperatures and heat capacity, entropy, enthalpy changes were fitted by quadratic formulas and the corresponding fitting factors ( $R^2$ ) were obtained as 0.9994, 0.9998 and 0.9999, respectively. The corresponding fitting equations and the correlation graphics of those shown in Fig. S10 are as follows.

$$\begin{aligned} C &= 4.74293 + 0.13657T - 5.1636 \times 10^{-5}T^2 & (R^2 = 0.9994) \\ S &= 58.7100 + 0.17965T - 5.4797 \times 10^{-5}T^2 & (R^2 = 0.9998) \\ H &= -0.51352 + 0.01327T + 4.8516 \times 10^{-5}T^2 & (R^2 = 0.9999) \end{aligned}$$

To have helpful information for the further study of E-6-CIN molecule, the thermodynamic data are presented. They can also be used to calculate the other thermodynamic energies according to relationships of thermodynamic functions and estimate directions of chemical reactions according to the second law of thermodynamics in thermochemical field. Notice that all thermodynamic calculations were done in gas phase and they could not be used in solution.

#### 4.5. Nonlinear optical properties and dipole moment

The electronic dipole moment, molecular polarizability, anisotropy of polarizability and molecular first hyperpolarizability of the molecule are calculated. The tensors of polarizability and hyperpolarizability ( $\alpha_{xx}, \alpha_{xy}, \alpha_{yy}, \alpha_{xz}, \alpha_{yz}, \alpha_{zz}$  and  $\beta_{xxx}, \beta_{xxy}, \beta_{xyy}, \beta_{yyy}, \beta_{xxz}, \beta_{xyz}, \beta_{yyz}, \beta_{xzz}, \beta_{yzz}, \beta_{zzz}$ ) can be caused by a frequency job output file of Gaussian.

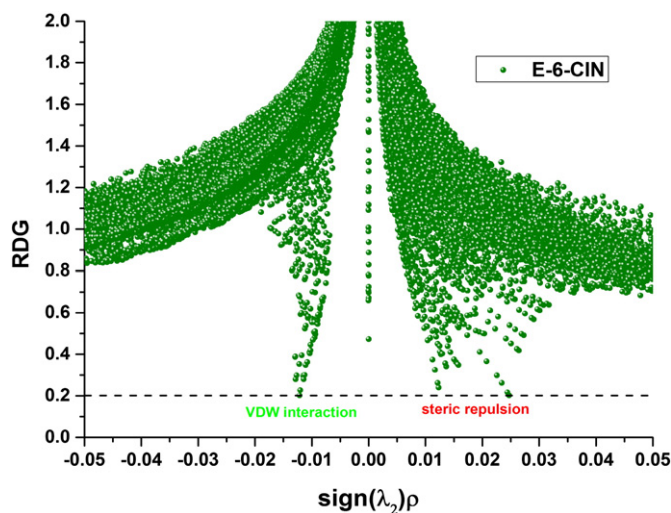


Fig. 9. The reduced density gradient for E-6-CIN molecule.

However, the values of  $\alpha$  and  $\beta$  in the Gaussian output are in atomic units (a.u.) so these values are converted into electronic units (esu) ( $\alpha; 1 \text{ a.u.} = 0.1482 \times 10^{-24} \text{ esu}$ ;  $\beta; 1 \text{ a.u.} = 8.6393 \times 10^{-33} \text{ esu}$ ).

The nonlinear optical parameters and electronic dipole moment  $\{\mu_i (i = x, y, z)\}$  and total dipole moment  $\mu_{tot}$  of the molecule are listed in Table S4. The total dipole moment also can be computed using the following equation.

$$\mu_{tot} = (\mu_x^2 + \mu_y^2 + \mu_z^2)^{\frac{1}{2}}$$

The higher values of dipole moment, molecular polarizability, and hyperpolarizability are significant for more active NLO properties. The E-6-CIN molecule has relatively homogeneous charge distribution and it does not have large dipole moment. The value of dipole moment is calculated as 2.4125 Debye (D). The calculated polarizability and anisotropy of the polarizability of the molecule are  $18.177017 \times 10^{-24}$  and  $48.337655 \times 10^{-24}$  esu, respectively. The value of the molecular

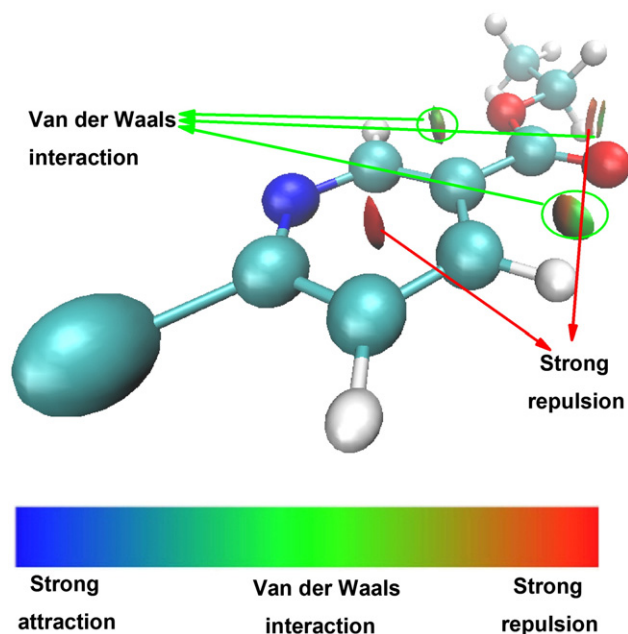


Fig. 10. The colored (blue–green–red scale) surfaces of E-6-CIN molecule according to values of sign  $\lambda_2$ .

hyperpolarizability,  $\beta$ , is one of the important key factors in an NLO system. The calculated first hyperpolarizability value ( $\beta$ ) of the molecule is equal to  $5916.104781 \times 10^{-33}$  esu. The first hyperpolarizability, polarizability, anisotropy of the polarizability and dipole moment values of the studied molecule are larger than those of urea which is one of the prototypical molecule used in the study of the NLO properties of molecular systems. Therefore E-6-CIN molecule is a good candidate of NLO material.

#### 4.6. Reduced density gradient – RDG

Johnson and co-workers [76] proposed an approach, named reduced density gradient (RDG), to explore weak interactions in real space based on the electron density and its derivatives. The RDG is

dimensionless quantity defined as, obtained density and its first derivative, follows:

$$RDG(r) = \frac{1}{2(3\pi^2)^{1/3}} \frac{|\nabla\rho(r)|}{\rho(r)^{4/3}}$$

The weak interactions are shown in the region with low electron density and low RDG. The electron density  $\rho$  (plot of the RDG versus) multiplied by the sign of  $\lambda_2$  can permit investigation and visualization of a wide range of interactions types. The sign of  $\lambda_2$  is used to discriminate bonded ( $\lambda_2 < 0$ ) from nonbonded ( $\lambda_2 > 0$ ) interactions. The RDG calculations are performed by Multiwfn [29], and plotted by VMD program [30], respectively.

**Table 7**  
NBO results showing formation of Lewis and non-Lewis orbitals for E-6-CIN.

Bond (A–B)	Type	ED (a.u.)	ED <sub>A</sub> (%)	ED <sub>B</sub> (%)	NBO	s (%)	p (%)
C1–C2	$\sigma$	1.974	48.92	51.08	0.6994(sp <sup>1.87</sup> )C+0.7147(sp <sup>1.89</sup> )C	34.89	65.07
		–0.729					
C1–C18	$\sigma$	1.972	49.76	50.24	0.7054 (sp <sup>1.79</sup> )C+0.7088(sp <sup>1.79</sup> )C	35.80	64.16
		–0.739					
C2–C3	$\sigma$	1.981	51.88	48.12	0.7203(sp <sup>1.87</sup> )C+0.6937(sp <sup>1.61</sup> )C	34.85	65.11
		–0.740					
C2–C8	$\sigma$	1.973	52.07	47.93	0.7216(sp <sup>2.28</sup> )C+0.6923(sp <sup>1.63</sup> )C	30.50	69.45
		–0.690					
C3–N20	$\sigma$	1.976	40.28	59.72	0.6347(sp <sup>2.16</sup> )C+0.7728(sp <sup>1.83</sup> )N	31.59	68.31
		–0.849					
C4–Cl7	$\sigma$	1.987	45.65	54.35	0.6756(sp <sup>3.28</sup> )C+0.7372(sp <sup>4.92</sup> )Cl	23.29	76.50
		–0.724					
C4–C18	$\sigma$	1.984	31.46	68.54	0.7070C(sp <sup>1.37</sup> )C+0.7072(sp <sup>1.95</sup> )C	42.20	57.76
		–0.760					
C4–N20	$\sigma$	1.988	40.83	59.17	0.6390(sp <sup>1.91</sup> )C+0.7692(sp <sup>1.70</sup> )N	34.38	65.53
		–0.894					
C8–O9	$\sigma$	1.995	35.26	64.74	0.5938(sp <sup>1.93</sup> )C+0.8046(sp <sup>1.45</sup> )O	34.11	65.74
		–1.102					
C8–O10	$\sigma$	1.992	31.44	68.56	0.5607(sp <sup>2.60</sup> )C+0.8280(sp <sup>2.07</sup> )O	27.74	72.01
		–0.941					
O10–C11	$\sigma$	1.989	69.87	30.13	0.8359(sp <sup>2.50</sup> )O+0.5489(sp <sup>4.16</sup> )C	30.86	68.92
		–0.825					
C11–C14	$\sigma$	1.990	50.70	49.30	0.7120(sp <sup>2.21</sup> )C+0.7022(sp <sup>2.48</sup> )C	31.12	68.84
		–0.647					
C1–C2	$\sigma^*$	0.021	51.08	48.92	0.7147(sp <sup>1.87</sup> )C – 0.6994(sp <sup>1.89</sup> )C	34.89	65.07
		0.537					
C1–C18	$\sigma^*$	0.016	50.24	49.76	0.7088(sp <sup>1.79</sup> )C – 0.7054(sp <sup>1.79</sup> )C	35.80	64.16
		0.557					
C2–C3	$\sigma^*$	0.031	48.12	51.88	0.6937(sp <sup>1.87</sup> )C – 0.7203(sp <sup>1.61</sup> )C	34.85	65.11
		0.537					
C2–C8	$\sigma^*$	0.066	47.93	52.07	0.6923(sp <sup>2.28</sup> )C – 0.7216(sp <sup>1.63</sup> )C	30.50	69.45
		0.400					
C3–N20	$\sigma^*$	0.015	59.72	40.28	0.7728(sp <sup>2.16</sup> )C – 0.6347(sp <sup>1.83</sup> )N	31.59	68.31
		0.513					
C4–C18	$\sigma^*$	0.038	42.20	57.76	0.7072(sp <sup>1.37</sup> )C – 0.7070(sp <sup>1.95</sup> )C	42.20	57.76
		0.522					
C4–N20	$\sigma^*$	0.032	59.17	40.83	0.7692(sp <sup>1.91</sup> )C – 0.6390(sp <sup>1.70</sup> )N	34.39	65.57
		0.524					
C8–O9	$\sigma^*$	0.019	64.74	35.26	0.8046(sp <sup>1.93</sup> )C – 0.5938(sp <sup>1.45</sup> )O	34.11	65.74
		0.589					
C8–O10	$\sigma^*$	0.096	68.56	31.44	0.8280(sp <sup>2.60</sup> )C – 0.5607(sp <sup>2.07</sup> )O	27.74	72.01
		0.351					
O10–C11	$\sigma^*$	0.033	69.87	30.13	0.5489 (sp <sup>2.50</sup> )O – 0.8359(sp <sup>4.16</sup> )C	28.58	71.37
		0.235					
C11–C14	$\sigma^*$	0.007	49.30	50.70	0.7022(sp <sup>2.21</sup> )C – 0.7120(sp <sup>2.48</sup> )C	31.12	68.84
		0.378					
Cl7	LP(1)	1.993	–	–	sp <sup>0.20</sup>	83.14	16.85
		–0.939	–	–	–	–	–
O9	LP(1)	1.979	–	–	sp <sup>0.69</sup>	59.28	40.70
		–0.716	–	–	–	–	–
O10	LP(1)	1.965	–	–	sp <sup>1.57</sup>	38.92	61.05
		–0.588	–	–	–	–	–
N20	LP(1)	1.898	–	–	sp <sup>2.59</sup>	27.81	72.10
		–0.364	–	–	–	–	–

The RDG of the molecule is plotted in Fig. 9. The RDG versus  $\text{sign}(\lambda_2)\rho$  peaks (electron density value) itself provides the information about the strength of interaction. The  $\text{RDG} = 0.2$  lines are evaluated in this molecule and crossed not only the attractive but also the repulsion spikes. Large, negative values of  $\text{sign}(\lambda_2)\rho$  are indicative of stronger attractive interactions (spikes in the left part in Fig. 9), while positive ones, strong repulsion interactions (spikes in the right part in Fig. 9). Values near zero indicated very weak Van der Waals interactions. The weak interaction region can be located by generating RDG isosurface enclosing the corresponding regions in the real molecular space (Fig. 10). The gradient isosurfaces are colored to the values of  $\text{sign}(\lambda_2)\rho$ , which is found to be a good indicator of interaction strength shown in Fig. 10. The color from blue to red means from stronger attraction to repulsion, respectively. The center of ring of the title molecule showed that strong steric effect, filled by red color. The green color circles can be identified as Van der Waals (VDW) interaction region, which means that density electron in these regions are low. The RDG of the molecule is contributed in the literature.

#### 4.7. Natural bond orbital (NBO) analysis

The most accurate possible “natural Lewis structure” picture of  $\phi$  is supplied NBO analysis, using the highest possible percentage of the electron density for all orbital details chosen mathematically. This analysis gives information about interactions in both occupied and unoccupied orbital spaces that could enhance the analysis of intra- and inter-molecular interactions. The interacting stabilization energy resulting from the second-order micro-disturbance theory and some electron donor orbital, acceptor orbital are published [77,78].

The second order Fock matrix (perturbation theory analysis) was carried out to determine the donor–acceptor interactions in NBO basis of the molecule. The results of interactions showed that in a loss of occupancy from the localized. NBO of the idealized Lewis structure into an empty non-Lewis orbital. For each donor ( $i$ ) and acceptor ( $j$ ), the

stabilization energy  $E^{(2)}$  associated with the delocalization  $i \rightarrow j$  is estimated as

$$E^{(2)} = \Delta E_{ij} = q_i \frac{F_{(i,j)}^2}{\varepsilon_i - \varepsilon_j}$$

where  $q_i$  is the donor orbital occupancy,  $\varepsilon_i$  and  $\varepsilon_j$  are diagonal elements and  $F_{(i,j)}$  is the off diagonal NBO Fock matrix element. An efficient method is NBO analysis for studying intra- and inter-molecular bonding, interaction among bonds and investigating charge transfer or conjugative interaction in molecular systems. Table 7 depicts the bonding concepts such as type of bond orbital, their occupancies, the natural atomic hybrids of which the NBO is composed, giving the percentage of the NBO on each hybrid, the atom label, and a hybrid label showing the hybrid orbital ( $sp^x$ ) composition (the amount of s-character, p-character, etc.) of E-6-CIN molecule. The larger  $E^{(2)}$  (energy of hyperconjugative interactions) value shows the intensive interaction between electron-donors and electron-acceptors i.e. the more donating tendency from electron donors to electron acceptors, and greater the extent of conjugation of the whole system, so the possible intensive interactions are given in Table 8.

The second-order perturbation theory analysis of Fock matrix in NBO basis shows strong intramolecular hyperconjugative interactions of electrons. The intramolecular interactions are formed by the orbital overlap between  $\sigma(\text{C—C})$ ,  $\sigma^*(\text{C—C})$ ,  $\pi(\text{C—C})$ ,  $\pi^*(\text{C—C})$  bond orbital which results intramolecular charge transfer (ICT) causing stabilization of the system. These interactions are observed as increase in electron density (ED) in C-C anti-bonding orbital that weakens the respective bonds. The electron density of conjugated bond of aromatic ring (ca. 1.99e) clearly demonstrates strong delocalization. The strong intramolecular hyper conjugation interaction of the  $\sigma$  and  $\pi$  electrons of C—C, C—H, C—N and C—Cl to the anti C—C, C—H and C—N bond leads to stabilization of some part of the ring as evident from Table 7.

**Table 8**  
Second order perturbation theory analysis of Fock matrix in NBO basis for E-6-CIN.

Donor ( $i$ )	Type	ED/e	Acceptor ( $j$ )	Type	ED/e	$E^{(2)a}$ (kcal mol <sup>-1</sup> )	$E(j)-E(i)^b$ (a.u.)	$F(i,j)^c$ (a.u.)
C1—C2	$\sigma$	1.974	C1—C18	$\sigma^*$	0.016	2.50	1.29	0.051
			C2—C3	$\sigma^*$	0.031	3.61	1.27	0.060
C1—C18	$\sigma$	1.972	C1—C2	$\sigma^*$	0.021	2.76	1.28	0.053
			C2—C8	$\sigma^*$	0.066	2.76	1.14	0.051
			C4—C17	$\sigma^*$	0.061	4.76	0.86	0.058
			C4—C18	$\sigma^*$	0.038	3.16	1.26	0.057
			C2—C3	$\pi^*$	0.321	16.25	0.29	0.061
C1—C18	$\pi$	1.651	C4—N20	$\sigma^*$	0.032	29.55	0.26	0.074
			C1—C2	$\sigma^*$	0.021	3.78	1.28	0.062
C2—C3	$\sigma$	1.981	C1—C18	$\pi^*$	0.016	22.98	0.29	0.074
C2—C3	$\pi$	1.626	C4—N20	$\pi^*$	0.427	16.40	0.25	0.059
			C8—O9	$\pi^*$	0.256	21.02	0.28	0.070
C2—C8	$\sigma$	1.973	O10—C11	$\sigma^*$	0.033	3.55	0.93	0.051
C3—N20	$\sigma$	1.976	C4—C17	$\sigma^*$	0.061	5.26	0.97	0.064
C4—C17	$\sigma$	1.987	C3—N20	$\sigma^*$	0.015	3.30	1.24	0.057
C4—N20	$\pi$	1.730	C1—C18	$\pi^*$	0.263	11.20	0.34	0.055
			C2—C3	$\pi^*$	0.321	24.86	0.34	0.083
C8—O9	$\pi$	1.983	C2—C3	$\pi^*$	0.321	4.18	0.40	0.040
C17	LP(3)	1.909	C4—N20	$\pi^*$	0.427	15.33	1.85	0.151
O9	LP(2)	1.850	C8—O10	$\sigma^*$	0.096	31.84	0.63	0.129
O10	LP(2)	1.791	C2—C8	$\sigma^*$	0.066	17.79	0.68	0.101
			C8—O9	$\pi^*$	0.256	47.13	0.34	0.114
N20	LP(1)	1.898	C4—C18	$\sigma^*$	0.038	10.50	0.89	0.087
C4—N20	$\pi^*$	0.032	C1—C18	$\pi^*$	0.263	95.02	0.03	0.082
			C2—C3	$\pi^*$	0.031	109.84	0.03	0.083

<sup>a</sup>  $E^{(2)}$  means energy of hyperconjugative interactions (stabilization energy).

<sup>b</sup> Energy difference between donor and acceptor  $i$  and  $j$  NBO orbitals.

<sup>c</sup>  $F(i,j)$  is Fock matrix element between  $i$  and  $j$  NBO orbitals.

The intramolecular hyperconjugative interaction of the  $\sigma(C1-C2)$  distributes to  $\sigma^*(C2-C3)$  and  $(C1-C18)$  leads to less stabilization of 3.61 and 2.50 kcal/mol, respectively; the  $\sigma(C1-C18)$  distributes to  $\sigma^*(C4-C17)$ ,  $(C4-C18)$ ,  $(C2-C8)$  and  $(C1-C2)$  4.76, 3.16, 2.76 and 2.76 kcal/mol, respectively; and the  $\sigma(C2-C3)$  distributes to  $\sigma^*(C1-C2)$  and leads to less stabilization as 3.78 kcal/mol. This enhanced further conjugate with anti-bonding orbital of  $\pi^*(C2-C3)$  and  $\sigma^*(C4-N20)$  which leads to strong delocalization of 16.25 and 29.55 kcal/mol, as shown in Table 8. This enhanced  $\pi^*(C1-C18)$  NBO further conjugates with  $\pi^*(C2-C3)$ , resulting in an enormous stabilization energy of 95.02 and 109.84 kcal/mol, as shown in Table 8. There occurs a strong intramolecular hyperconjugative interaction, from  $LP(3) C17 \rightarrow \pi^*(C4-N20)$  and  $LP(2) O10 \rightarrow \pi^*(C8-O9)$  which increases ED (1.909e and 1.791e) that weakens the respective bonds leading to stabilization of 15.33 and 47.13 kcal/mol, respectively. The increased electron density at the chlorine atom leads to the elongation of C—Cl bond and a lowering of the C—Cl stretching wavenumber. The electron density is transferred from the n(Cl) to the anti-bonding  $\sigma$  orbital of the C—C bond, explaining both the elongation and the red shift [79]. The C—N stretching mode can be used as a good probe for evaluating the bonding configuration around the N atom and the electronic distribution of the ring. The n- $\pi$  conjugation between the nitrogen lone pair electrons and ring system is strong in the ground state [79]. In this paper, the  $LP(1)-(N20) \rightarrow \sigma^*(C4-C18)$  energies are 10.50 kcal/mol, showing n-conjugation between N and ring.

## 5. Conclusion

The spectroscopic properties of E-6-CIN molecule, such as optimized parameters, vibrational assignments, magnetic properties and some electronic properties, are investigated. The vibrational (FT-IR and FT-Raman) spectra of E-6-CIN are obtained with experimental and theoretically and the fundamental modes are assigned using their PED. NMR spectra of the molecule are recorded in DMSO solution and the chemical shifts of hydrogen and carbon atoms are evaluated for solvent effects. Some electronic properties are given such as: the frontier molecular, HOMO and LUMO orbitals, density of states, MEPs and Mulliken charges of the molecule. The thermodynamic properties are evaluated and the results are increasing with temperature. Nonlinear optical properties, reduced density gradient and natural bond orbital analysis of E-6-CIN molecule are investigated and gained to the literature. The results are prepared and it showed an acceptable good agreement with the experimental data.

## Acknowledgement

This work was supported by the Celal Bayar University Research fund through research Grant No.: FBE-2011/70.

## Appendix A. Supplementary data

Supplementary data to this article can be found online at <http://dx.doi.org/10.1016/j.saa.2015.09.007>.

## References

- [1] R. Chuck, Appl. Catal. A Gen. 280 (2005) 75–82.
- [2] E. Cronin, R.B. Stoughton, Arch. Dermatol. 87 (1963) 445–449.
- [3] M.A. Goher, Q.C. Yang, T.C. Mak, Polyhedron 19 (2000) 615–621.
- [4] J. Moncol, M. Palicová, P. Segla, M. Koman, M. Melník, M. Valko, T. Glowiak, Polyhedron 21 (2002) 365–370.
- [5] R.K. Sivamani, B. Stoeber, G.C. Wu, H. Zhai, D. Liepmann, H. Maibach, Skin Res. Technol. 11 (2005) 152–156.
- [6] M. Kržič, M. Sentjurc, J. Kristl, J. Control. Release 70 (2001) 203–211.
- [7] H. Zhai, J.P. Ebel, R. Chatterjee, K.J. Stone, V. Gartstein, K.D. Juhlin, A. Pelosi, H.I. Maibach, Skin Res. Technol. 8 (2002) 13–18.
- [8] L.M. Buckmiller, J.P. Lapointe, R.A. Ludwig, J. Bacteriol. 173 (1991) 2017–2025.
- [9] R. Świsłocka, E. Regulska, M. Samsonowicz, W. Lewandowski, Polyhedron 28 (2009) 3556–3564.
- [10] P. Koczoń, J. Piekut, M. Borawska, W. Lewandowski, J. Mol. Struct. 651–653 (2003) 651–656.
- [11] P. Koczoń, J. Piekut, M. Borawska, R. Świsłocka, W. Lewandowski, Spectrochim. Acta A 61 (2005) 1917–1922.
- [12] P. Koczoń, T. Hrynaskiewicz, R. Świsłocka, M. Samsonowicz, W. Lewandowski, Vib. Spectrosc. 33 (2003) 215–222.
- [13] W. Lewandowski, B. Dasiewicz, P. Koczoń, J. Skierski, K. Dobrosz-Teperek, R. Świsłocka, L. Fuks, W. Priebe, A. Mazurek, J. Mol. Struct. 604 (2002) 189–193.
- [14] Y. Xu, L.L. Yang, S.Y. Yang, J. Liu, Acta Crystallogr. Sect. E Struct. Rep. Online 68 (2012) o162.
- [15] P. Hohenberg, W. Kohn, Phys. Rev. 136 (1964) B864–B871.
- [16] A.D. Becke, J. Chem. Phys. 98 (1993) 5648–5652.
- [17] C. Lee, W. Yang, R.G. Parr, Phys. Rev. B 37 (1988) 785–789.
- [18] M. Frisch, G.W. Trucks, H.B. Schlegel, G.E. Scuseria, M.A. Robb, J.R. Cheeseman, G. Scalmani, V. Barone, B. Mennucci, G.A. Petersson, others, Inc., Wallingford, CT (2009).
- [19] N. Sundaraganesan, S. Ilakiamani, H. Saleem, P.M. Wojciechowski, D. Michalska, Spectrochim. Acta A 61 (2005) 2995–3001.
- [20] M.H. Jamróz, Spectrochim. Acta A 114 (2013) 220–230.
- [21] R. Dennington, T. Keith, J. Millam, GaussView, Version 5, 2009.
- [22] R. Ditchfield, J. Chem. Phys. 56 (1972) 5688–5691.
- [23] K. Wolinski, J.F. Hinton, P. Pulay, J. Am. Chem. Soc. 112 (1990) 8251–8260.
- [24] M. Petersilka, U.J. Gossmann, E.K.U. Gross, Phys. Rev. Lett. 76 (1996) 1212–1215.
- [25] M. Karabacak, L. Sinha, O. Prasad, Z. Cinar, M. Cinar, Spectrochim. Acta A 93 (2012) 33–46.
- [26] R. Bauernschmitt, R. Ahlrichs, Chem. Phys. Lett. 256 (1996) 454–464.
- [27] C. Jamorski, M.E. Casida, D.R. Salahub, J. Chem. Phys. 104 (1996) 5134–5147.
- [28] N.M. O'boyle, A.L. Tenderholt, K.M. Langner, J. Comput. Chem. 29 (2008) 839–845.
- [29] T. Lu, F. Chen, J. Comput. Chem. 33 (2012) 580–592.
- [30] W. Humphrey, A. Dalke, K. Schulten, J. Mol. Graph. 14 (1996) 33–38.
- [31] E.D. Glendening, A.E. Reed, J.E. Carpenter, F. Weinhold, NBO Version 3.1, 1998.
- [32] B.G. Johnson, P.M.W. Gill, J.A. Pople, J. Chem. Phys. 98 (1993) 5612–5626.
- [33] P.A. Papanikolaou, P.C. Christidis, A.T. Chaviara, C.A. Bolos, A.C. Tsipis, Eur. J. Inorg. Chem. 2006 (2006) 2083–2095.
- [34] M. Karabacak, M. Çinar, M. Kurt, J. Mol. Struct. 885 (2008) 28–35.
- [35] M. Karabacak, M. Kurt, Spectrochim. Acta A 71 (2008) 876–883.
- [36] M.V.N. de Souza, S.M.S.V. Wardell, R.A. Howie, Acta Crystallogr. Sect. E Struct. Rep. Online 61 (2005) o1347–o1349.
- [37] S. Long, M. Siegler, T. Li, Acta Crystallogr. Sect. E Struct. Rep. Online 63 (2006) o279–o281.
- [38] D.E. Lynch, I. McClenaghan, Acta Crystallogr. Sect. E Struct. Rep. Online 58 (2002) o708–o709.
- [39] D. Sajan, N. Vijayan, K. Safakath, R. Philip, M. Karabacak, Spectrochim. Acta A 108 (2013) 197–210.
- [40] P.B. Nagabalasubramanian, M. Karabacak, S. Periandy, J. Mol. Struct. 1017 (2012) 1–13.
- [41] M. Karabacak, S. Bilgili, A. Atac, Spectrochim. Acta A 135 (2015) 270–282.
- [42] E. Kose, F. Bardak, A. Atac, M. Karabacak, M.A. Cipiloglu, Spectrochim. Acta A 114 (2013) 38–45.
- [43] R.M. Silverstein, F.X. Webster, D.J. Kiemle, Spectrometric Identification of Organic Compounds, John Wiley & Sons, 2005.
- [44] B.H. Stuart, Infrared Spectroscopy: Fundamentals and Applications, Wiley, 2004.
- [45] M. Govindarajan, K. Ganasan, S. Periandy, M. Karabacak, S. Mohan, Spectrochim. Acta A 77 (2010) 1005–1013.
- [46] N.B. Colthup, L.H. Daly, S.E. Wiberley, Introduction to Infrared and Raman Spectroscopy, Academic Press, 1990.
- [47] G. Socrates, Infrared and Raman Characteristic Group Frequencies: Tables and Charts, John Wiley & Sons Ltd., West Sussex, England, 2001.
- [48] F.R. Dollish, W.G. Fateley, F.F. Bentley, Characteristic Raman Frequencies of Organic Compounds, Wiley, 1974.
- [49] V. Karunakaran, V. Balachandran, Spectrochim. Acta A 128 (2014) 1–14.
- [50] M. Govindarajan, M. Karabacak, Spectrochim. Acta A 96 (2012) 421–435.
- [51] G. Varsányi, Assignments for Vibrational Spectra of Seven Hundred Benzene Derivatives, Halsted Press, 1974.
- [52] M. Karabacak, E. Kose, A. Atac, Spectrochim. Acta A 91 (2012) 83–96.
- [53] N. Sundaraganesan, C. Meganathan, B. Anand, B.D. Joshua, C. Lapouge, Spectrochim. Acta A 67 (2007) 830–836.
- [54] M. Karabacak, M. Cinar, S. Ermeç, M. Kurt, J. Raman Spectrosc. 41 (2010) 98–105.
- [55] E.F. Mooney, Spectrochim. Acta 20 (1964) 1021–1032.
- [56] M. Arivazhagan, D. Anitha Rexalin, Spectrochim. Acta A 96 (2012) 668–676.
- [57] M. Arivazhagan, R. Kavitha, J. Mol. Struct. 1011 (2012) 111–120.
- [58] A. Atac, M. Karabacak, C. Karaca, E. Kose, Spectrochim. Acta A 85 (2012) 145–154.
- [59] A. Atac, M. Karabacak, E. Kose, C. Karaca, Spectrochim. Acta A 83 (2011) 250–258.
- [60] A. Nataraj, V. Balachandran, T. Karthick, M. Karabacak, A. Atac, J. Mol. Struct. 1027 (2012) 1–14.
- [61] O. Sala, N. Gonçalves, L. Noda, J. Mol. Struct. 566 (2001) 411–416.
- [62] Z. Cinar, M. Karabacak, M. Cinar, M. Kurt, P. Chinna Babu, N. Sundaraganesan, Spectrochim. Acta A 116 (2013) 451–459.
- [63] P.B. Nagabalasubramanian, M. Karabacak, S. Periandy, Spectrochim. Acta A 85 (2012) 43–52.
- [64] N. Sundaraganesan, S. Ilakiamani, B. Dominic Joshua, Spectrochim. Acta A 68 (2007) 680–687.
- [65] S. Muthu, E.I. Paulraj, Spectrochim. Acta A 112 (2013) 169–181.
- [66] N. Subramanian, N. Sundaraganesan, J. Jayabharathi, Spectrochim. Acta A 76 (2010) 259–269.



- [67] M. Cinar, M. Karabacak, Spectrochim. Acta A 104 (2013) 428–436.
- [68] K. Pihlaja, E. Kleinpeter, Carbon-13 NMR Chemical Shifts in Structural and Stereochemical Analysis, VCH, 1994.
- [69] H.O. Kalinowski, S. Berger, S. Braun, Carbon-13 NMR Spectroscopy, 1988.
- [70] K. Fukui, Science 218 (1982) 747–754.
- [71] C.H. Choi, M. Kertesz, J. Phys. Chem. A 101 (1997) 3823–3831.
- [72] R.G. Parr, R.G. Pearson, J. Am. Chem. Soc. 105 (1983) 7512–7516.
- [73] R.G. Parr, W. Yang, Density-Functional Theory of Atoms and Molecules, Oxford University Press, USA, 1989.
- [74] M. Chen, U.V. Waghmare, C.M. Friend, E. Kaxiras, J. Chem. Phys. 109 (1998) 6854–6860.
- [75] J.S. Murray, Molecular Electrostatic Potentials: Concepts and Applications, Elsevier, 1996.
- [76] E.R. Johnson, S. Keinan, P. Mori-Sanchez, J. Contreras-Garcia, A.J. Cohen, W. Yang, (2010) 6498–6506.
- [77] M. Szafran, A. Komasa, E. Bartoszak-Adamska, J. Mol. Struct. 827 (2007) 101–107.
- [78] C. James, A.A. Raj, R. Reghunathan, V.S. Jayakumar, I.H. Joe, J. Raman Spectrosc. 37 (2006) 1381–1392.
- [79] S. Sudha, N. Sundaraganesan, M. Kurt, M. Cinar, M. Karabacak, J. Mol. Struct. 985 (2011) 148–156.